Spring 1957

The mechanism of energy dissipation in the hydraulic jump

S. Nagaratnam
University of Iowa

THE MECHANISM OF ENERGY DISSIPATION IN THE HYDRAULIC JUMP

134

by

S. Nagaratnam

A thesis submitted in partial fulfillment of the requirements for the degree of Master of Science, in the Department of Mechanics and Hydraulics, in the Graduate College of the State University of Iowa

June, 1957

Chairman: Professor Hunter Rouse

1610

This thesis is hereby approved as a creditable report on an engineering project or research carried out and presented in a manner which warrants its acceptance as a prerequisite for the degree for which it is submitted. It is to be understood, however, that neither the Department of Mechanics and Hydraulics nor the thesis adviser is responsible for the statements made or for the opinions expressed.

Thesis Adviser

Head of the Department

ACKNOWLEDGMENT

The writer is grateful to Dr. T. T. Siao for explaining his thesis and for his help during the initial stages of the work. His derivations of the momentum and energy equations for the hydraulic jump have been adopted in this work.

Special thanks are due to Dr. Hunter Rouse for his patient guidance and encouragement and to Dr. P. G. Hubbard for his enthusiastic and ready help whenever there was trouble with electronic instruments.

The writer is also thankful to Dr. Richard Lloyd-Jones of the Technical Writing Department for reading the manuscript and to Mrs. Inez Mortley for typing the thesis.

This study was partially supported by the Office of Naval Research through contract N8onr500(03) with the Iowa Institute of Hydraulic Research.

TABLE OF CONTENTS

TABLE OF FIGURES

NOTATION

Time means are indicated by bar over the symbols. A repetition of indices indicates summation. Notations which are not listed here are defined in the text or by a definitive sketch. Repetition of x, y, z directions is indicated by i .

A	Surface area
d	Depth of flow; d_1 and d_2 refer to initial and final sections, respectively
F	Froude number $U_1/\sqrt{gd_1}$
g	Gravitational acceleration
K	Similarity factor for the structure of small eddies
l	Length of roller
L	Length of the hydraulic jump
n	Unit vector normal to a surface element pointing away from the region
p	Instantaneous pressure intensity
p'	Fluctuating component of p
R	Reynolds number $U_1 d_1/\nu$
S	Distance along the surface
t	Time
U_1	Space mean of $\bar{u}$ for the initial section
u	Instantaneous velocity

u'	Fluctuating component of u
$\bar{u},\bar{v},\bar{w}$	Time means of velocity components for rectangulate coordinates in the direction of x, y and z, respectively
u',v',w'	Corresponding components of the fluctuating component of velocity
$\forall$	Body volume
W	Weber number $u_1/\sqrt{\sigma/\rho d_1}$
y	Depth
ρ	Density
γ	Specific weight
μ	Dynamic viscosity
ν	Kinematic viscosity
σ	Surface tension
Δ	Indicates change in value from that of the initial section - e.g. $\Delta p = p - p_1$

Chapter I

INTRODUCTION

It is well known that the hydraulic jump causes a considerable amount of energy loss. But little has been known about the exact mechanism of energy dissipation, though sufficient experimental values of the total loss of energy are available. Development in both the theory of turbulence and the experimental measurement of various turbulence characteristics has now made it possible to analyse the various factors which cause this energy loss.

In turbulent flow past a wall, mean energy is transformed into turbulent energy at a certain rate. This transfer of mean energy occurs through the production of eddies, which are initially concentrated in the region of steep velocity gradient near the wall. The vertical fluctuating components of the turbulent and mean velocities carry these eddies to regions of lower eddy concentration where they are disintegrated into smaller eddies and eventually lose their kinetic energy in the form of heat. Hence a considerable amount of turbulent energy is dissipated away from the essential zone of turbulence generation. Without such a transport of turbulent energy, loss due to turbulence might be entirely different.

Rollers play an important part in the production, transport, and dissipation of turbulent energy. If one can obtain a change in depth of flow from subcritical to supercritical without causing a hydraulic jump, it becomes evident how much less is the loss of energy [6].

The high shear along the interface between the roller and the expanding jet causes the creation of eddies. The effectiveness of the roller depends upon its length, the relative high shear along the interface, and the vertical transport of momentum. All these quantities increase with the increasing Froude number.

Because the motion in the hydraulic jump is essentially turbulent, understanding the mechanism of motion and energy dissipation requires that one find experimentally the various characteristics of the hydraulic jump at different Froude numbers. The presence of many air bubbles in a jump formed in water makes difficult the use of the hot-film anemometer for turbulence measurement. But the absence of such a hetrogeneous feature and the suitability of the hot-wire anemometer for the measurement of turbulence, make it possible to study this problem in an air-flow model.

Because the close similarity of the mean flow patterns between the hydraulic jump formed in water and the one similated in air had been already demonstrated by T. T. Siao [1], no attempt was made to rerun the experiment in water except to find the length of roller and the ratio of initial and final depths, for they are important factors in establishing surface profiles in the air model (Fig. 2).

In this work, after the surface profile was adjusted for the required Froude number, the mean flow pattern was worked out from the velocity profiles measured at different sections. By means of the equation of continuity the vertical component of mean velocity was calcu-

lated. The various characteristics of turbulence $\sqrt{\overline{u'^2}}$, $\sqrt{\overline{v'^2}}$, $\overline{u'v'}$, and $\overline{(\partial u'/\partial t)^2}$ were measured with the hot-wire anemometer; the values are graphically presented. The production and dissipation of turbulent energy was calculated for various points. Also the momentum and energy equations were derived and their experimental values worked out for Froude numbers 2 and 6.

In the latter part of this thesis, wherever necessary, values of various characteristics worked out for $F = 2$ and $F = 6$ have been compared with those of Siao. Values for $F = 4$ have been taken from his thesis [1] and for $F = 8$ from his data sheets.

Chapter II

SIMILITUDE

In the dimensional analysis of the hydraulic jump, if the variables involved are ρ, g, μ, H_L, U_1, σ, and d_1, then

$$\frac{H_L}{U_1^2/2g} = f(F, R, W)$$

The test results of the hydraulic jump indicate that the loss of total energy depends only on F, the resistance of the boundaries being small. Also W can be dropped as the capillary effects are negligible. On the other hand, for the same boundary profile in air and water, if the Reynolds number is high, then the law of similitude for hydrostatic pressure distribution is

$$\left(\frac{p_1 - p_2}{U_1^2/2g}\right)_a = \left(\frac{p_1 - p_2}{U_1^2/2g}\right)_w$$

Since in air γh is very small, and in water $h = d$

$$\left(\frac{p_1 - p_2}{\rho U_1^2/2}\right)_a = \left(\frac{d_1 - d_2}{U_1^2/2g}\right)_w$$

But

$$\frac{d_1 - d_2}{U_1^2/2g} = \frac{2(d_1 - d_2)}{F^2 d_1}$$

Therefore,

$$\frac{\Delta \bar{p}}{\rho U_1^2/2} = \frac{2\Delta d}{F^2 d_1} \qquad (1)$$

Equation (1) implies that if the air duct is run with water, the free surface of the jump will coincide with the adjustable boundary of the air model and the pressure along the boundary will be zero. But the very nature of instability of the free surface in a true hydraulic jump makes such an exact similitude questionable. It was found during the

experiment in the air model that the length of roller was smaller than that of the true hydraulic jump. Because the roller plays a vital part in the production and dissipation of turbulent energy, it was considered that the length of the roller should be maintained equal to that of the true hydraulic jump. It was possible to accomplish that by slightly changing the inlet angle in the adjustable boundary. Since the straight portion following the bell-mouthed entrance was only 2 1/2" wide, it was not possible to measure the angle of entrance, δ, accurately. The position where the chances that a piece of string attached to an end of a thin rod might point either upstream or downstream were equal was considered to be the end of the roller.

In addition to the lack of similarity between the air model and the true hydraulic jump, as indicated above, one cannot ignore the following obvious limitations:-

1. The very presence of an additional boundary alters both the pressure and velocity distribution in the flow.

2. Though the growth of the boundary layer in the adjustable boundary is retarded by the presence of the roller in the initial length of jump, yet the affect of the boundary layer beyond the roller has been neglected.

3. The instability of the free surface cannot be similated in air-flow model.

4. The presence of air bubbles in the true hydraulic jump makes it markedly different from the homogeneous nature of the air-flow model.

In spite of all these limitations, the convenience and availability of suitable turbulence-measuring instruments made the air model the choice for the study of this problem.

Chapter III

THEORETICAL CONSIDERATIONS

The continuity equation and the Navier-Stokes equation for incompressible flow in tensor notation are

$$\frac{\partial u_\kappa}{\partial x_\kappa} = 0 \tag{2}$$

$$\frac{\partial u_i}{\partial t} + u_\kappa \frac{\partial u_i}{\partial x_\kappa} = -\frac{1}{\rho}\frac{\partial p}{\partial x_i} + \nu \frac{\partial^2 u_i}{\partial x_\kappa \partial x_\kappa} \tag{3}$$

For turbulent flow where $u = \bar{u} + u'$ and $p = \bar{p} + p'$ the Navier-Stokes equation takes the form

$$\frac{\partial}{\partial t}(\bar{u}_i+u') + (\bar{u}_\kappa+u'_\kappa)\frac{\partial}{\partial x_\kappa}(\bar{u}_i+u'_i) = -\frac{1}{\rho}\frac{\partial(\bar{p}+p')}{\partial x_i} + \nu\frac{\partial^2(\bar{u}_i+u'_i)}{\partial x_\kappa \partial x_\kappa} \tag{4}$$

Since $\overline{\partial u_k/\partial x_k} = 0$, $\overline{\partial u'_k/\partial x_k} = 0$, $\overline{u'_1} = 0$, and $\overline{p'} = 0$ when the time average of Eq. (4) is considered, it reduces to

$$\frac{\partial \bar{u}_i}{\partial t} + \bar{u}_\kappa \frac{\partial \bar{u}_i}{\partial x_\kappa} + \overline{u'_\kappa \frac{\partial u'_i}{\partial x_\kappa}} = -\frac{1}{\rho}\frac{\partial(\bar{p}+\gamma h)}{\partial x_i} + \nu \frac{\partial^2 \bar{u}_i}{\partial x_\kappa \partial x_\kappa} \tag{5}$$

This is the Reynolds equation.

Volume integration of Eq. (5) gives

$$\rho\int\frac{\partial \bar{u}_i}{\partial t}d\forall + \rho\int\bar{u}_\kappa\frac{\partial \bar{u}_i}{\partial x_\kappa}d\forall + \rho\int\overline{u'_\kappa\frac{\partial u'_i}{\partial x_\kappa}}d\forall = -\int\frac{\partial(\bar{p}+\gamma h)}{\partial x_i}d\forall + \mu\int\frac{\partial^2 \bar{u}_i}{\partial x_\kappa \partial x_\kappa}d\forall \tag{6}$$

Green's theorem states that

$$\int\frac{\partial M}{\partial x_i}d\forall = \int n_i M dS \tag{7}$$

in which n_1 are the direction cosines of a unit normal vector at surface element dS and the positive direction of the normal is understood

to be outward from the surface; M is a function of x, y, and z. Then, applying Eq. (7) to Eq. (6),

$$\rho\int\frac{\partial\bar{u}_i}{\partial t}\,d\forall + \rho\int\bar{u}_i\bar{u}_k n_k\,dS + \rho\int\overline{u_i'u_k'}\,n_k\,dS =$$

$$-\int\bar{p}\,n_i\,dS - \int\tau\hbar\,n_i\,dS + \mu\int\frac{\partial\bar{u}_i}{\partial x_k}n_k\,dS \qquad (8)$$

Since $\int\tau\hbar n_i\,dS = 0$, as τ is very small for air, and $\int\frac{\partial\bar{u}_i}{\partial t}\,d\forall = 0$ for steady flow, Eq. (8) reduces to

$$\rho\int\bar{u}_i\bar{u}_k n_k\,dS + \rho\int\overline{u_i'u_k'}\,n_k\,dS = -\int\bar{p}\,n_i\,dS + \mu\int\frac{\partial\bar{u}_i}{\partial n_k}n_k\,dS \qquad (9)$$

This is the general equation of momentum for steady flow. The physical meanings of the terms in the Eq. (8) are,

$\rho\int\frac{\partial\bar{u}_i}{\partial t}\,d\forall$ — Rate of change of momentum in the region.

$\rho\int\bar{u}_i\bar{u}_k n_k\,dS$ — Rate of out flow of momentum through the surface of the region due to the mean motion.

$\rho\int\overline{u_i'u_k'}\,n_k\,dS$ — Total Reynolds stresses on the surface of the region due to the superposed turbulent motion.

$-\int n_i(\bar{p}+\tau\hbar)\,dS$ — Total pressure acting on the surfaces of the region.

$\mu\int n_k\frac{\partial\bar{u}_i}{\partial x_k}dS$ — Total viscous shear on the surface of the region.

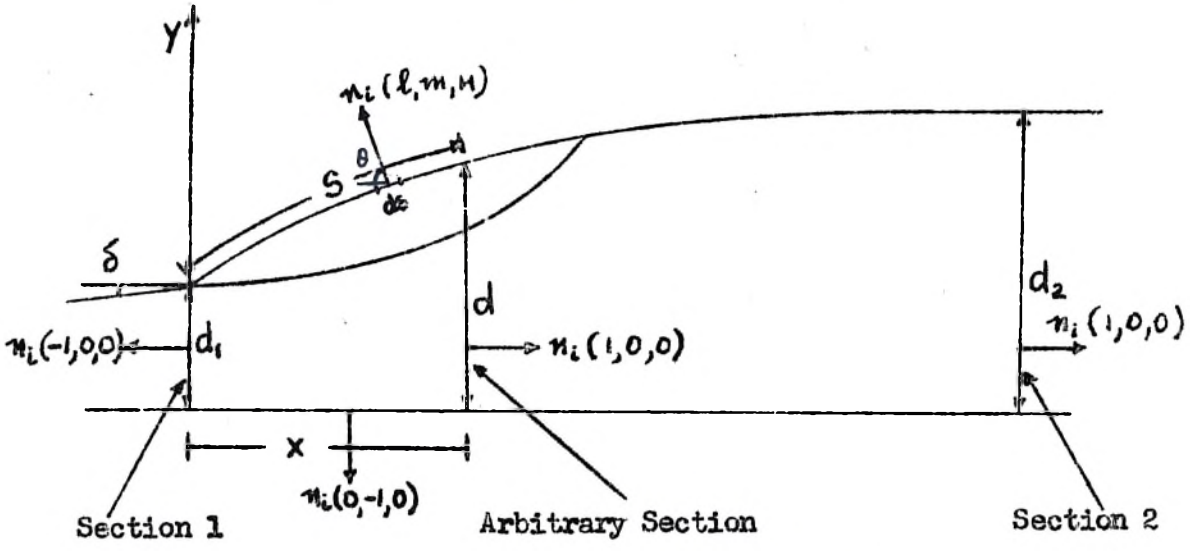

Definition sketch for nomenclature

Applying Eq. (9) to the problem under consideration according to the accompanying sketch and dividing the resultant equation by $\rho U_1^2 d_1$ to make it dimensionless, one gets

$$\int_0^{d_1}\left(\frac{\bar{u}}{U_1}\right)^2\frac{dy}{d_1} + \int_0^{d_1}\frac{\overline{u'^2}}{U_1^2}\frac{dy}{d_1} =$$

$$\frac{1}{\rho U_1^2 d_1}\left(\bar{p}d - \bar{p}d_1 - \int_{d_1}^{d}\bar{p}_x\cos\theta\,ds\right) + \int_0^{d}\left(\frac{\bar{u}}{U_1}\right)^2\frac{dy}{d_1} + \int_0^{d}\frac{\overline{u'^2}}{U_1^2}\frac{dy}{d_1} - \frac{1}{R}\int\frac{\partial \bar{u}/U_1}{\partial n}\,ds \qquad (10)$$

where, according to Eq. (1),

$$\frac{1}{\rho U_1^2 d_1}\left(\bar{p}d - \bar{p}d_1 - \int_{d_1}^{d}\bar{p}_x\cos\theta\,ds\right) = \frac{1}{2F^2}\left(\frac{d^2}{d_1^2} - 1\right)$$

The first two terms of Eq. (10) are the rate of flow of momentum in the x-direction caused by the mean motion and the superposed turbulent motion at the initial section 1. The third term represents the

net total pressure on the region considered. The fourth and the fifth terms have the same meaning as the first and second terms, respectively, for an arbitrary section. The last term represents the shear along all the boundaries.

Energy Equation

To obtain the energy equation for the mean motion, for the growth of turbulence, the Navier-Stokes equations are multiplied by the mean velocity components.

Multiplying Eq. (5) with $\rho \bar{u}_i$ and taking rh $\doteq$ 0 we get

$$\frac{\rho}{2}\frac{\partial}{\partial t}(\bar{u}_i\bar{u}_i) + \frac{\rho}{2}\frac{\partial}{\partial x_k}(\bar{u}_i\bar{u}_i\bar{u}_k) + \rho\bar{u}_i\,\overline{u'_k\frac{\partial u'_i}{\partial x_k}} =$$

$$-\bar{u}_i\frac{\partial \bar{p}}{\partial x_i} + \mu\,\bar{u}_i\frac{\partial^2\bar{u}_i}{\partial x_k\partial x_k} \qquad (11)$$

Upon carrying out volume integration of this equation and making suitable transformation one obtains

$$\frac{\partial}{\partial t}\int\frac{\rho\bar{u}_i^2}{2}d\forall + \frac{\rho}{2}\int\bar{u}_i^2\bar{u}_k n_k dS + \rho\int\bar{u}_i n_k\overline{u'_i u'_k}dS + \rho\int\overline{u'_i u'_k}\frac{\partial\bar{u}_i}{\partial x_k}d\forall =$$

$$-\int\bar{p}\bar{u}_i n_i dS + \mu\int\left(\frac{\partial\bar{u}_i}{\partial x_k} + \frac{\partial\bar{u}_k}{\partial x_i}\right)\bar{u}_i n_k dS - \mu\int\left(\frac{\partial\bar{u}_i}{\partial x_k} + \frac{\partial\bar{u}_k}{\partial x_i}\right)\frac{\partial\bar{u}_i}{\partial x_k}d\forall \qquad (12)$$

The physical meaning of each term in Eq. (12) is as follows:

$\frac{\partial}{\partial t}\int\frac{\rho\bar{u}_i^2}{2}$ — Rate of local changes of mean energy in the volume of fluid considered.

$\frac{\rho}{2}\int \bar{u}_i^2 \bar{u}_K n_K dS$ — Rate of convection of mean energy through the surface of the volume.

$\rho\int \bar{u}_i n_K \overline{u_i' u_K'} dS$ — Rate of work done on the surface by Reynolds stresses.

$\rho\int \overline{u_i' u_K'} \frac{\partial \bar{u}_i}{\partial x_K} d\forall$ — Rate of work done in the volume of fluid by Reynolds stresses, or production of turbulent energy.

$-\int \bar{p}\, \bar{u}_i n_i dS$ — Rate of work done by mean pressure acting on the surface of the fluid volume.

$\mu\int\left(\frac{\partial \bar{u}_i}{\partial x_K} + \frac{\partial \bar{u}_K}{\partial x_i}\right)\bar{u}_i n_K dS$ — Rate of work done by mean viscous shear stress on the surface of the volume of fluid.

$-\mu\int\left(\frac{\partial \bar{u}_i}{\partial x_K} + \frac{\partial \bar{u}_K}{\partial x_i}\right)\frac{\partial \bar{u}_i}{\partial x_K} d\forall$ — Rate of work done by mean viscous stress in the volume or dissipation of energy due to mean motion.

For the present study $\frac{\partial}{\partial t}\int \frac{\rho \bar{u}_i^2}{2} d\forall = 0$ because the flow is steady.

Assuming $\frac{\partial \bar{p}}{\partial y} = 0$, Eq. (12) reduces to

$$\int_0^{d_1}\left(\frac{\bar{u}}{U_1}\right)^3 \frac{dy}{d_1} + 2\int_0^{d_1}\frac{\bar{u}}{U_1}\left(\frac{\overline{u'^2}}{U_1^2}\right)\frac{dy}{d_1} = \underbrace{\frac{\Delta \bar{p}}{\rho U_1^2/2}}_{\text{I}} + \underbrace{\int_0^{d}\frac{\bar{u}}{U_1}\frac{(\bar{u}^2+\bar{v}^2)}{U_1^2}\frac{dy}{d_1}}_{\text{II}}$$

$$\underbrace{2\int_0^{d}\left(\frac{\bar{u}}{U_1}\frac{\overline{u'^2}}{U_1^2} + \frac{\bar{v}}{U_1}\frac{\overline{u'v'}}{U_1^2}\right)\frac{dy}{d_1}}_{\text{III}} - \underbrace{2\int_0^{x}\int_0^{d}\left[\left(\frac{\overline{u'^2}-\overline{v'^2}}{U_1^2}\right)\frac{\partial \bar{u}/U_1}{\partial x} + \frac{\overline{u'v'}}{U_1^2}\left(\frac{\partial \bar{u}/U_1}{\partial y} + \frac{\partial \bar{v}/U_1}{\partial x}\right)\right]\frac{dx}{d_1}dy}_{\text{IV}}$$

$$-\frac{2}{R}\int_0^d\left[2\frac{\bar{u}}{U_1}\frac{\partial \bar{u}/U_1}{\partial x}+\frac{\bar{v}}{U_1}\left(\frac{\partial \bar{u}/U_1}{\partial y}+\frac{\partial \bar{v}/U_1}{\partial x}\right)\right]dy+\frac{2}{R}\int_0^x\int_0^d\left[4\left(\frac{\partial \bar{u}/U_1}{\partial x}\right)^2+\left(\frac{\partial \bar{u}/U_1}{\partial y}+\frac{\partial \bar{v}/U_1}{\partial x}\right)^2\right]dx\,dy$$

V VI

(13)

The terms in the left-hand side of the above equation represent the rate of convection of energy due to mean motion and the rate of work done by Reynold stresses at the initial section. The terms in the right hand side of the equation represent, in order, (I) the rate of work done by mean pressure, (II) the rate of convection of mean energy, (III) the rate of work done by Reynolds stresses on the surface, (IV) the rate of production of turbulent energy, (V) the work done by mean viscous stresses, and (VI) the rate of viscous dissipation in the region. Thus the total energy at the initial section is accounted for at any section.

To obtain the energy equation due to turbulent motion for the decay of turbulence, Eq. (5) is multiplied by $\rho\, u_i'$ and volume integration carried out. Then one gets, taking $rh = 0$,

$$\frac{\partial}{\partial t}\int\frac{\rho}{2}\overline{u_i'u_i'}\,d\forall+\int\frac{\rho}{2}\overline{u_i'u_i'}\,u_k n_k\,ds+\rho\int n_k\,\overline{u_i'u_i'u_k'}\,ds$$

$$+\int\rho\overline{u_i'u_k'}\frac{\partial \bar{u}_i}{\partial x_k}\,d\forall=-\int\overline{u_i'p'}\,n_i\,ds+$$

$$\mu\int\overline{\left(\frac{\partial u_i'}{\partial x_k}+\frac{\partial u_k'}{\partial x_i}\right)u_i'}\,n_k\,ds-\mu\int\overline{\left(\frac{\partial u_i'}{\partial x_k}+\frac{\partial u_k'}{\partial x_i}\right)\frac{\partial u_i}{\partial x_k}}\,d\forall \qquad (14)$$

In the above equation for the turbulent motion each term carries the same physical meaning as the corresponding one of Eq. (12), except the third term from the left. It represents the rate of diffusion of tur-

bulent energy.

Applying Eq. (14) to the two-dimensional, steady flow under consideration one gets

$$-2\int_0^x\int_0^d \frac{\overline{u_i' u_k'}}{U_1^2}\frac{\partial \overline{u_i}/U_1}{\partial x_k}\frac{dy\,dx}{d_1} = \Delta\int_0^d \frac{\overline{u'p'}}{\rho U_1^{3/2}}\frac{dy}{d_1} + \Delta\int_0^d \frac{\overline{u}}{U_1}\frac{(\overline{u'^2}+\overline{v'^2}+\overline{w'^2})}{U_1^2}\frac{dy}{d_1}$$

$$\text{IV} \qquad\qquad 1 \qquad\qquad 2$$

$$+\Delta\int_0^d \frac{\overline{u'(u'^2+v'^2+w'^2)}}{U_1^3}\frac{dy}{d_1} + \Delta\,\frac{2}{R}\int_0^d\left[\frac{\partial}{\partial x}\left\{\frac{(\overline{u'^2}+\overline{v'^2}+\overline{w'^2})}{2U_1^2} + \frac{\overline{u'^2}}{U_1^2}\right\} + \frac{\partial}{\partial y}\frac{\overline{u'v'}}{U_1^2}\right]dy \qquad (15)$$

$$3 \qquad\qquad\qquad\qquad\qquad\qquad 5$$

$$+\frac{2}{R}\int_0^x\int_0^d K\left(\frac{\partial u'/U_1}{\partial x}\right)^2 dy\,dx$$

$$4$$

where

$$K = \frac{\mu\int\overline{\left(\frac{\partial u_i'}{\partial x_k}+\frac{\partial u_k'}{\partial x_i}\right)\frac{\partial u_i}{\partial x_k}}\,d\forall}{\mu\int\overline{\left(\frac{\partial u'}{\partial x}\right)^2}\,d\forall}$$

and Δ indicates a change in value from that of initial section. Considering the entire length of jump, the term on the left-hand side means the total production of turbulent energy. The terms on the right-hand side mean, in order, (1) the rate of work done by p', (2) the rate of convection of turbulent energy, (3) the rate of diffusion of turbulent energy, (4) the rate of total dissipation of turbulent energy for the total length of jump, (5) the rate of work done by turbulent viscous stress with respect to initial section.

When the terms in the above equations of energy and momentum are computed from experimental data, the distribution of energy due to both mean motion and turbulent motion can be visualized over the entire region of transition.

Chapter IV

EQUIPMENT AND TESTING PROCEDURE

Air Duct and Pressure Measurement

The experiments to obtain the data required for the foregoing analysis were conducted in a specially built air duct 2.5 feet wide (photo 1). It consisted of a bell-mouthed entrance, a short straight approach channel, a test section, and a tail piece leading to the suction side of a centrifugal blower. The centrifugal blower was run by a 3-hp induction motor of constant speed. The velocity in the duct could be varied by adjusting a butterfly valve placed just at the end of the air duct.

The bell-mouthed entrance was 1 1/2 feet long, consisting of four sides, each shaped according to a 2-to-1 ellipse. It was followed by straight approach section 2 1/2 inches long. The test section, which was 9 feet long, consisted of a fixed straight top boundary, two side walls - one of transparent lucite and the other of wood - and a curved adjustable boundary to represent the free surface of the true hydraulic jump. It was constructed upside down for the convenience of taking measurements. On the inside of the side wall made of wood, scales were marked up to 0.02 foot to facilitate adjustment of the curved boundary. The curved boundary made of 1/8-inch-thick lucite could be adjusted by varying the height of struts attached to it. The tail piece consisted of a straight passage 4 feet long, followed by a 3 1/2-foot converging channel which ended in a foot-long cylindrical piece. The butterfly

valve was located in the cylindrical piece attached to the inlet of the blower.

At the outlet of the blower was fixed a diverging truncated cone 2 1/2 feet long with an end diameter of 1 foot. From the velocity profiles measured along two diameters at right angles to each other, the discharge was calculated by integration. For velocity measurement a Prandtl-type Pitot tube with a velocity coefficient of unity was used. During calibration for discharge, the pressure reading for each discharge was measured at a piezometric hole provided at the base of the cone. The values are presented in Fig. 1.

Pressure in the test section was measured with the piezometric holes provided along the central line of the upper straight boundary and the bottom curved boundary at 6 inches interval. Because there was no difference of pressure between the upper and lower boundary at a section, pressure was measured only along the lower boundary. An improved Wahlen gage of 0.001-inch-of-alcohol accuracy was used for pressure measurement.

Mean Velocity Measurements

The selection of a proper instrument to measure mean velocity was important for the flow was turbulent and curvilinear. Conventional Pitot tubes measure dynamic pressure when held opposite in the direction of flow; such Pitot tubes cannot respond to negative velocities as they respond to positive velocities because of their asymmetry about the vertical axis. Therefore, none of the conventional Pitot tubes such as Prantdl, Brabbee, etc., could be used. Hence a Cole type of instrument consisting

of two tubes pointing in opposite directions and an electrical hot-wire anemometer were possible alternatives. The latter indicates maximum velocity at a point irrespective of direction, and the former responds to the direction of flow and is sensitive to the reverse velocity field. That advantage made the Cole tube a better choice.

The instrument used for the present experiment was made of hyperdermic needles with an inside diameter of 0.04 inch. The two tips were 0.6 inch apart. The pitometer was calibrated by mounting it in a jet, at different velocities and at different angles of inclination, θ. The downstream tube registers a negative pressure, for its outlet is in the wake of the upstream tube. Therefore, when $\theta = 0^{\circ}$ the pressure difference registered by the two tubes of the pitometer for a mean velocity $\bar{u}$ is greater than $\rho u^2/2$. If a factor k were introduced to take care of the discrepancy, then the relationship would be

$$\rho \frac{\bar{u}^2}{2} = \frac{\Delta \bar{p}}{K} \qquad (K>1) \tag{16}$$

the value of k for different velocities is plotted in Fig. 3a. Then the velocity of jet is kept constant and the pitometer rotated through different angles. As previously the pitometer would indicate a higher pressure difference. If $\bar{u}$ is the x-component of $\bar{U}$ then

$$\rho \frac{\bar{U}^2}{2} = \frac{\Delta \bar{p}}{K'} \qquad (K'>1)$$

But

$$\bar{u} = \bar{U} \cos\theta$$

$$\rho \frac{\bar{u}^2}{2} = \frac{\Delta \bar{p} \cos^2\theta}{K'} \tag{17}$$

Refer to Fig. 3b for the variation of $\cos^2\theta/k'$ with respect to θ.

For measuring $\bar{u}$ in the air duct, the pitometer was oriented along the x-direction in the flow and the pressure difference measured. Since the correction for the direction of flow cannot be applied unless the direction of velocity is known, first it was assumed $\theta = 0^\circ$ and $\bar{u}$ calculated - i.e., only the correction as indicated in Eq. (16) was applied. Based on the tentative value of $\bar{u}$ the stream function for the flow was calculated and the corresponding flow pattern plotted. From the inclination of the stream lines the direction of flow, which was only approximate, was found out for any point. Then the correction for inclination Eq. (17) was applied and a new $\bar{u}$ calculated and a second stream function drawn. It was found that there was not sufficient appreciable difference between the first and the second mean flow patterns to warrant repetition of the above procedure.

Turbulence Measurements

The quantities $\overline{u'^2}$, $\overline{v'^2}$, $\overline{u'v'}$, and $\overline{(\partial u'/\partial t)^2}$ were measured with a constant-temperature hot-wire anemometer having linearized characteristics. The cross-wire technique was adopted for measurement. The x-wire was made of two wires inclined at 45° to the direction of flow as indicated in the sketch and about 1/8 inch apart. The tungsten wire used

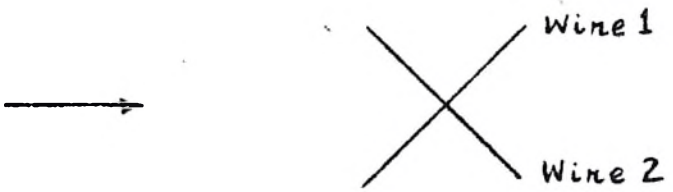

Definition sketch for cross-wire anemometer

was 0.00014 inch in diameter and had 2400 ohms resistance per foot length. It was copper plated in copper sulphate solution and soldered onto the probe. The coated copper was then etched away by nitric acid until 0.025 inch was exposed so that 5 ohms of electrical resistance was caused. The calibration of this wire was made in a uniform flow. Various amounts of current required to maintain constant temperature for different velocities were noted. The velocity of flow was calculated by using a standard Prantdl Pitot tube. As expected, the calibration curve was linear. Since the tungsten wire was slender, it was often broken during the course of experiment. Everytime that a new wire was fixed, it was calibrated.

The following equations were used in calculating turbulence characteristics:

$$\sqrt{\overline{u'^2}} = \frac{AC}{2\,Sin\theta} I_{TA} \qquad (18)$$

$$\sqrt{\overline{v'^2}} = \frac{AC}{2\,Cos\theta} I_{TB} \qquad (19)$$

$$\overline{u'v'} = \frac{A^2 B^2 \left(I_{T1}^2 - I_{T2}^2\right)}{4\,Sin\theta\,Cos\theta} \qquad (20)$$

$$\sqrt{\overline{\left(\frac{\partial u'}{\partial t}\right)^2}} = \frac{AD}{2\,Sin\theta} I_{D1} \qquad (21)$$

where θ Angle between the wire and the direction of flow = 45°

A Calibration constant = U/I

B Amplification constant

C Circuit constant

D Differential circuit constant

I_{T1}, I_{T2} Direct r.m.s. readings from wires 1, 2, respectively

I_{TA} I_{TB} r.m.s. readings through adding and subtracting circuits respectively.

Measurement of Local Rate of Energy Dissipations

The measured time rate of energy dissipation (Eq. 21) was converted to a spatial derivative by the following relation:

$$\overline{\left(\frac{\partial u'}{\partial x}\right)^2} = \frac{1}{\bar{u}^2}\overline{\left(\frac{\partial u'}{\partial t}\right)^2}$$

It was assumed that $\bar{u} \gg \bar{v}$ and $\bar{u}\,\partial u'/\partial x \gg u_i\,\partial \bar{u}/\partial x_i$

Since it was found that $\overline{w'^2}$ was very nearly equal to $\overline{v'^2}$ at all sections, no attempt was made to measure $\overline{w'^2}$ independently. Wherever it was necessary, it was assumed that $\overline{w'^2} = \overline{v'^2}$.

Chapter V

EXPERIMENTAL RESULTS AND DISCUSSION

In model testing one is often forced to choose between the importance of gravitational effects and that of viscous effects. Often one effect is ignored in favor of the other, depending upon the nature of the problem. For the problem under study, such a method cannot be adopted, for viscosity plays an important role in the dissipation of turbulent energy, and the predominance of gravitational effects cannot be ignored. Hence one has to take into consideration both the Froude and the Reynolds criteria. But, fortunately, the effect of viscosity on the mean flow is negligible if the Reynolds number is high. Therefore, not only were the geometric ratios maintained (Fig. 2) and F held constant for the hydraulic jumps in water and air, the experiments were run at high R . The experiments conducted in water for the determination of d_2/d_1 and ℓ/d_1, ratios were run between the Reynolds number 4.6×10^4 and 1.03×10^5 . The present experiments in the air model were also kept in the same range from 5.88×10^4 to 1.15×10^5 .

Profile Adjustments

In the air model because d_2 was fixed at 1 foot, to maintain the d_2/d_1 ratio for different values of F , the initial depth d_1 had to be varied. For F = 2 and 6 , d_1 was equal to 0.432 foot and 0.133 foot, respectively. The initial depth of flow was fixed so the adjustable boundary (similar to the free surface in the true hydraulic jump) was varied to satisfy Eq. (1). Although Eq. (1) was satisfied,

the length of roller was not equal to that measured in the actual hydraulic jump. It was smaller. It was possible to get the required length by slightly inclining one face of the 2 1/2-inch approach section. It could be assumed that the angle of inclination was less than 3°.

Between the surface profile as measured by the writer and the profile for $F = 4$ got by T. T. Siao [1], there is a maximum discrepancy of 8% at $x/y-y_1 = 2.5$. As in the water measurement, it seems, no two profiles presented by different people agree one with another. Considering the pressure fluctuation (analogous to free-surface fluctuation in water) such a variation is not too great. Also the effect of velocity distribution at the entrance section due to the presence of the 2-foot entrance section in the previous experiment might have had some influence on the surface profile. The trend is consistent when the surface profiles are presented in dimensionless form (Fig. 4). The length of jump varies from $8.75(y_2-y_1)$ for $F = 2$ to $6.25(y_2-y_1)$ for $F = 6$. Also it can be recalled that "the profile of water flow was slightly higher than that of air flow, probably because the air bubbles in the hydraulic jump caused the mean density to be smaller and the apparent piezometric head accordingly higher" [1].

Stream Function

The method of calculating the stream function has already been discussed in the previous chapter. Figures 5(a) and 5 portray the stream functions for $F = 2$ and 6, respectively. The line $\Psi / U_1 d_1 = 1$ divides the roller from the main flow. The length of roller is the same as in

the water measurement. The spacing between the stream lines at the upper and lower boundaries is larger because of the presence of the boundary layer.

Profiles of $\bar{u}/U_1$

The x-component of the mean velocity for different sections has been plotted in Figs. 6(a) and 6 for $F = 2$ and 6, respectively. All those curves have been superimposed in Figs. 7(a) and 7 to indicate the gradual variation in velocity profiles, which is, evidently, a good check on the experimental values. It was found that towards the end of the jump the discharge across a section calculated from the measured values of $\bar{u}$ had a maximum difference of +4.4% and +5.17% for $F = 6$ and 2, respectively. This was obviously due to the growth of boundary layer on all four sides of the air duct. The amount of discrepancy was considered small and, as it was necessary to maintain continuity relationship at every section, the measured values of $\bar{u}$ were proportionately reduced to represent the same rate of flow as at the initial section. Also are presented $\bar{u} = 0$, $\Psi/U_1 d_1 = 0$ in the figures. The curve $\bar{u} = 0$ is the locus of maximum Ψ. The line of $\partial \bar{u}/\partial y = 0$ has been drawn only for $F = 6$. Because the lines for $\partial \bar{u}/\partial y = 0$ for $F = 2$, and $\partial^2 \bar{u}/\partial^2 y = 0$ for both Froude numbers were difficult to define, they were not included.

The superimposed velocity profiles at the end sections indicate that the absolute magnitude of the velocity gradient is lower at the curved boundary than at the fixed boundary. This is caused by the delay in boundary-layer development due to the presence of the roller on the curved boundary.

The maximum negative values of $\bar{u}/U_1$ are 0.164, 0.23 and, 0.265 for $F = 2$, 4, and 6, respectively.

The profile for $F = 2$ and 6 at the entrance section varies markedly from that of $F = 4$ because of the presence of a 2 feet long entrance channel in the latter experiment compared to 2 1/2 inches long channel in the former.

Profiles of $\bar{v}/U_1$

Figures 8(a) and 8 represent $\bar{v}/U_1$ profiles for $F = 2$ and 6. Also $\bar{u} = 0$ and $\bar{v} = 0$ are plotted. The y-component of mean velocity, $\bar{V}$, was calculated directly from the continuity relationship

$$\frac{\bar{V}}{U_1} = \int \frac{\partial \bar{u}/U_1}{\partial x} dy$$

From the values of $\bar{u}/U_1$ profiles, $\bar{u}/U_1$-vs-x graph was drawn. In that graph the slope of every point at a particular section was measured and a $\partial\bar{u}/U_1\partial x$ -vs-y graph was drawn for that section. The graph of the summation of $\partial\bar{u}/U_1\partial x$ upto any point gives the value of $\bar{v}/U_1$ at that point. The maximum value of $\bar{v}/U_1$ occurs just at the end of the roller where the mean flow is highly curvilinear. The maximum values of $\bar{v}/U_1$ are 0.05, 0.079, 0.085, 0.105 for $F = 2$, 4, 6, 8 respectively. Too much accuracy cannot be expected of the above values for they involve a large number of slope measurements. Towards the end of the jump, $\bar{v}$ approaches zero. The intersection of $\bar{u} = 0$ and $\bar{v} = 0$ gives the center of the roller in each case. They divide the secondary flow into four parts, each having a particular velocity direction.

Turbulence Characteristics

The root-mean-square of the fluctuating component of velocity is a measure of turbulence. The experimental values of $\sqrt{\overline{u'^2}}/U_1$, $\sqrt{\overline{v'^2}}/U_1$, are presented in Figs. 9a and 9 for F = 2 and 6, respectively. At the entrance section, the intensity of turbulence is comparatively very small except at the boundaries. The maximum intensity of turbulence occurs about the middle section of the roller. At each succeeding section, as the eddies are carried across to the regions of low eddy concentration, the intensity of turbulence becomes more nearly uniform and smaller in magnitudes. Curves of $\partial\sqrt{\overline{u'^2}}/\partial y = 0$ are also drawn. The quantity $\sqrt{\overline{v'^2}}$ is always less than $\sqrt{\overline{u'^2}}$. Because there was not much difference between $\overline{v'^2}$ and $\overline{w'^2}$, wherever necessary they were taken as equal in the calculations.

The ratio between the velocity correlation and the square of the mean velocity at Section 1 is presented in Figs. 10(a) and 10. Also presented is $\overline{u'v'}/U_1^2 = 0$. As expected it nearly coincides with the $\partial\bar{u}/U_1\partial y = 0$ curve. For F = 2, the curve $\overline{u'v'}/U_1^2 = 0$ was not attempted for it was difficult to define accurately. The maximum values of $\overline{u'v'}/U_1^2$ occur along the first half of the interface between the roller and the jet.

The average of maximum values of $\sqrt{\overline{u'^2}}/U_1$, $\sqrt{\overline{v'^2}}/U_1$, and $\overline{u'v'}/U_1^2$, are presented in Fig. 11.

Production and Dissipation of Turbulent Energy

If the flow is laminar, the work done by external force on a fluid element is transformed into thermal energy because of the internal viscous stresses of the fluid element; thus, energy loss occurs locally. But in the turbulent flow, except for a small portion in the laminar boundary layer, the energy 'lost' to the mean flow is not dissipated locally. This loss of energy to the mean flow appears in the form of eddies which are the main source of turbulence. For example, in pipe flow, this generation of eddies occurs mainly in the narrow region along the wall, and as they become concentrated and unstable, they are carried into the central zone by the radial component of the fluctuating turbulent velocity. Various theories have been put forth to describe this diffusion process; but it is obvious that, if the flow is to maintain its turbulent characteristics, this transport process should be continuous. The eddies thus diffused throughout the entire cross section break up into smaller eddies and eventually lose their energy in the form of heat due to viscous attrition along their path of travel. Naturally, during the process of transport some energy will be lost because of viscous affects. In addition, if there is any loss of energy locally during the generation process, a positive difference between the dissipation and production of turbulent energy should show up.

The presence of the roller entirely alters the pattern of production and dissipation of turbulent energy from the simple case of pipe flow and thus can be analysed only experimentally. The local rate of turbulent energy production in its dimensionless form is $-2\frac{\overline{u_i' u_k'}}{U_1^2}\frac{\partial \bar{u}_i}{\partial x_k}\frac{d_1}{U_1}$

and it is equal to

$$-\left[\left(\frac{\overline{u^2}-\overline{v^2}}{U_1^2}\right)\frac{\partial \bar{u}/U_1}{\partial x} + \frac{\overline{u'v'}}{U_1^2}\left(\frac{\partial \bar{u}/U_1}{\partial y} + \frac{\partial \bar{v}/U_1}{\partial x}\right)\right]\frac{dx\,dy}{d_1}$$

The presence of the term $\overline{u'v'}/U_1^2(\partial\bar{u}/U_1\partial y)$ indicates that high rate of production of turbulence should occur near the fixed boundary where the velocity gradient is high and in the regions where turbulent shear velocity (Reynolds stresses) is high. The other three terms contribute only a little to the local production of turbulence. The measured values of the above expressions plotted in Figs. 12(a) and 12 for $F = 2$ and 6, respectively, clearly show the two distinct zones of production, one along the straight boundary and the other along the lower edge of the roller.

The general expression for the mean rate of viscous dissipation is

$$\bar{W} = \mu\left[2\overline{\left(\frac{\partial u'}{\partial x}\right)^2} + 2\overline{\left(\frac{\partial v'}{\partial y}\right)^2} + 2\overline{\left(\frac{\partial w'}{\partial z}\right)^2} + \overline{\left(\frac{\partial v'}{\partial x} + \frac{\partial u'}{\partial y}\right)^2} + \overline{\left(\frac{\partial w'}{\partial y} + \frac{\partial v'}{\partial z}\right)^2} + \overline{\left(\frac{\partial u'}{\partial z} + \frac{\partial w'}{\partial x}\right)^2}\right]$$

Because it was found that the three measured values of $\overline{(\partial u'/\partial x)^2}$, $\overline{(\partial v'/\partial y)^2}$, $\overline{(\partial w'/\partial x)^2}$ were nearly equal [1], the above expressions for dissipation reduce to

$$\bar{W} = 15\,\mu\overline{\left(\frac{\partial u'}{\partial x}\right)^2}$$

The local rate of turbulent energy dissipation is plotted in Figs. 12(a) and 12 for $F = 2$ and 6, respectively, in the dimensionless form $2/R\ K\overline{(\partial u'/\partial x)^2}d_1^2/U_1^2$. The value of K is evaluated by equating both

the production and the dissipation of turbulent energy for the entire jump. The dissipation is concentrated in the lower half of the roller in the beginning and eventually, due to diffusion, it is spread more in the y-direction and becomes uniform towards the end. The maximum dissipation curve is higher than the maximum production curve, indicating that the maximum production occurs along the lower edge of the roller and the maximum dissipation occurs in the lower half of the roller. Such a shift in the maximum dissipation curve may be due to the vertical component of the mean velocity in the region of curvilinear flow. Thus the local rates of production and dissipation are not equal in this case. Both the production and the dissipation of turbulent energy almost reach their minimum value in the upper half of the roller. This may be due to the effect of reverse flow. The slow rate of dissipation with decreasing F, it is believed, may be due to the decreasing scale of turbulence with increasing F.

The values of K are found to be 12.2, 13.5, 15 and 15 for $F = 2, 4, 6,$ and 8, respectively. For isotropic turbulence $K = 15$. Such increasing value of K with increasing F and values less than 15 may lead one to the following conclusions: -1. The turbulence tends to become isotropic with increasing F. 2. There may be loss due to the generation of turbulence. These conclusions may be far-fetched, for the experimental error has been completely ignored. It is assumed that $\overline{(\partial u'/\partial x)^2}$ includes the local loss due to generation. Such an assumption is questionable, as $\overline{(\partial u'/\partial x)^2}$ measures essentially the loss due to viscous attrition - not due to generation. Loss due to generation

should be the direct outcome of the Reynolds stresses. But, anyhow, at present we have neither a mathematical expression to include such a term nor an instrument to measure such a hypothetical quantity.

Momentum Balance

The momentum inflow at any section of a closed body is equal to the momentum outflow at another section minus the net total force acting on the body in the direction of flow between the two sections. The left-hand side of Eq. (10) gives the total inflow of momentum at the initial section and in its dimensionless form should be nearly equal to 1. The experimental values of terms right of the equality sign are plotted in Figs. 13(a) and 13 for $F = 2$ and 6, respectively.

Curve I shows net normal pressure between the initial section and any arbitrary section. Because the pressures on the curved and straight boundary were found to be practically equal, the measured values of pressure along the curved boundary were used. Also is plotted in the same figure the value of $\frac{1}{2F^2}\left(\frac{d^2}{d_1^2}-1\right)$. If the pressure along the curved boundary agreed with the condition given by Eq. (1), both the curves should completely coincide; the lack of coincidence can be attributed to experimental error.

In curve II is plotted the total flux of momentum due to the mean motion in the x-direction. It has a value slightly higher than 1 at the initial section, probably because of the velocity distribution at that section. Its decrease from its maximum value is slowed down by the presence of roller. The minimum values are 0.13, 0.22, and 0.45 for

$F = 2$, 4, and 6, respectively. The deviation of the above values from their respective ratios of d_2/d_1 is an indication of a lack of vertical constancy of $\bar{u}$. This deviation seems to increase with decreasing F for approximately the same R.

In curve III is plotted the total flux of momentum due to turbulent motion in the x-direction. It attains its maximum value about $x = \ell$. For $F = 2$, the maximum value is comparatively low. But the ratio between the minimum and the maximum values is high, indicating that the decay of turbulence is at a lower rate.

Because the mean velocity has not been measured close enough to the boundary to evaluate correctly $\partial\bar{u}/\partial y$, the shear force along the boundary is not calculated. But one would expect that when the sum of curves I, II, and III is subtracted from the total momentum at the initial section, the difference should be equal to the shear force. But, surprisingly, the difference does not increase with the length of jump. It has its maximum value at the end of the roller, thereafter gradually decreasing to a minimum value at the end of the jump. The deviation at the end of the jump is equal to 2% and 9% for $F = 2$ and 6, respectively. From measurement in water it was found that $D/\rho U_1^2 d_1$ was equal to 4.2% and 8.2% for $F = 2$ and 6. [1]

Mean Energy Balance

The experimental values of each term in the right side of the equality sign of Eq. (13) are plotted separately in Fig. 14(a) and 14 for $F = 2$ and 6, respectively. A composite plot of all the curves is

also presented in Figs. 15(a) and 15.

Curve I shows the rate at which work is done by the mean pressure, which increases in the x-direction depending upon the rate of expansion of the jet. Since it is the same as the left hand side of Eq. (1), for comparison the value of $2\Delta D/F^2 d_1$ is also plotted. The two curves differ slightly throughout the length of the jump for $F = 6$, upto $x = \ell$ for $F = 4$, and in the middle portion for $F = 2$. These discrepancies can be attributed only to experimental error. It attains the maximum value at the end section where mean velocity is the minimum. The maximum values are 0.65, 0.48, and 0.38 for $F = 2$, 4 and 6 respectively.

In Curve II is plotted the total rate of convection of the mean energy. It decreases in the x-direction more rapidly than the rate of change of momentum due to the mean motion, as the latter is a function of $(\bar{u}/U_1)^2$ while the former $(\bar{u}/U_1)^3$. The value greater than 1 at the initial section can be attributed, as before, only to the non-uniform velocity distribution. It has as its minimum values 0.21, 0.05 and 0.02 for $F = 2$, 4, and 6, respectively, indicating that the drain on the mean convective energy increases with increasing F.

In Curve III is plotted the rate at which work is done by the Reynolds stresses. Work done by these apparent stresses is the cause of production of turbulent energy - i.e., formation of large eddies. The Reynolds stresses can be visualized as shear stress resulting from the transport of momentum across the flow due to the turbulent velocity in a

flow having normal mean velocity gradient. If there is no mean velocity gradient across the flow, there can be no Reynolds stresses and consequently no conversion of mean energy into turbulent energy. This process can be clearly verified in the case of $F = 2$, where at the first few sections $\partial\bar{u}/\partial y = 0$. At this point, it should not be forgotton that the Reynolds stresses which are obtained by grouping certain accelerative terms with viscous terms is simply a convenient way to illustrate the net effect turbulent velocity has on the flow, as the instantaneous viscous stresses disappear through the averaging process in the analysis. Both the Reynold stresses and the production of turbulent energy are two aspects of the same phenomenon, although the work done by the former is conservative and the latter eventually disappears as heat due to viscosity. It is worth noting that the Reynold stresses may be quite large compared to the mean viscous shear.

Curve III has its maximum value in the second half of the roller and is equal to 0.04, 0.095 and 0.13 for $F = 2$, 4, and 6, respectively.

In Curve IV is plotted the production of turbulent energy. Curve A, which is the total amount of production of turbulent energy upto a section, is got by integrating Curve IV. The rate of production is higher at the beginning - approaching a maximum in the first half of the roller and then decreasing gradually. At the end of the roller nearly 50%, 87%, and 90% of total turbulent energy for $F = 2$, 4, and 6, respectively, has been produced. The low value for $F = 2$ may be due to the comparetively small roller and the high ratio between the minimum

and the maximum turbulent intensity in the jump.

Curve V represents the rate at which work is done by mean viscous stresses and is in the order of 10^{-5} . It is conservative and, as pointed out before, it is very small compared to the Reynolds stresses.

Curve VI represents dissipation due to the mean motion and it is in the order of 10^{-3} . Also is plotted the cumulative value of the above dissipation along the x-direction. The magnitude of total dissipation increases with increasing F . Both these terms (V and VI) are analogous to the Reynolds stresses and the production of turbulent energy in a broad sense. But it should be clearly distinguished that because mean viscous stresses are real, dissipation of energy due to them results directly in the formation of heat, and because Reynold stresses are fictitious, the work done by them goes into the production of eddies. Finally, the eddies lose their energy in the form of heat due to viscosity. It is worth noting that the viscosity plays no direct part in causing the Reynold stresses.

As the values of the terms V and VI are very small, they can be neglected if R is high. Hence the values of other four terms are plotted together in Fig. 15(a) and 15. If the effects of the terms V and VI are ignored the discrepancy at the end section is 7% and 7.5% for F = 2 and 6, respectively. I + II + III + IV has its minimum value at $x = \ell$ and increases afterwards. Maybe decreasing turbulent energy after $x = \ell$ causes such an increase in the sum of four terms.

Turbulent Energy Balance

The energy equation for the turbulent motion in the problem under study has been derived in the form of Eq. (15). In that equation the value of each term is expressed with respect to its value at the initial section for the convenience of plotting. The close resemblence between both the energy equations, which have the production of energy term in common, can be noted.

Term IV in the left-hand side of Eq. (15) represents the total production of turbulent energy. Terms 1 and 3 representing work done by p' and diffusion of turbulent energy, respectively, cannot be calculated, because the pressure-velocity correlation, $\overline{u'p'}$, and the triple velocity correlation cannot be measured. Term 2, which gives the convection of turbulent energy, has been plotted in Figs. 16(a) and 16. As values of work done by the viscous stresses are very low, no attempt has been made to plot those values.

Curve 4, representing dissipation of turbulent energy, attains its maximum value towards the end of the roller. The rate of increase of Curve 4 is lower than that of Curve IV, representing the production of turbulent energy. Curve B represents the total dissipation of turbulent energy upto a section. The constant, K, was calculated by equating the total production and the dissipation of turbulent energy.

The comparison of curves A and B shows the relatively high rate of production with respect to dissipation upto the end of the roller. In the case of $F = 2$, this tendency persists for a longer distance due

to the low rate of decay of turbulence.

The sum of terms 1 and 3 can be arrived at by subtracting term 2 from the difference of terms 4 and IV, as term 5 can be neglected. This has been attempted in Figs. 15(a) and 15. The sum (1 + 3) has a negative value for $F = 2$ throughout the entire length of the jump except at $x = 0$; for $F = 4$, it has its negative value in between, having both the ends zero; for $F = 6$, the first half of the jump, it has negative values and for the second half of the jump it has positive values, both ends being zero. However, the value of (1 + 3) is very small.

CONCLUSION

From the experimental work on the hydraulic jump for Froude numbers 2, 4, and 6 simulated in a duct with air as fluid medium, the following conclusions can be arrived at:

1. The hydraulic jump can be simulated in an air duct with good approximation. Since for any given mean-flow pattern the distribution of the turbulence characteristics is unique, the turbulence measurements for the simulated jump should apply with the same degree of approximation to the actual jump. [1]

2. (a) The average ratio of intensity of turbulence to the initial mean velocity increases with F.

(b) In the first half of the roller along the interface between the roller and the expanding jet, the maximum value of the ratio between the intensity of turbulence and the mean velocity at the initial section occurs. The ratio has maximum values of 0.195, 0.24, and 0.29 for $F = 2$, 4, and 6. It approaches the minimum value of the uniform flow at the end of the jump, where it is equal to 0.05, 0.045, and 0.035 for $F = 2$, 4, and 6.

3. (a) Along the interface between the roller and the expanding jet, the production of turbulent energy is concentrated. The ratio between the length of interface and the initial depth increases with F. Hence the production of turbulent energy with respect to the kinetic energy at the initial section increases with F.

(b) Before the end of the roller, the major portion of the

production and dissipation of turbulent energy occurs.

(c) The maximum-dissipation curve is at a higher elevation than the maximum-production curve. This is due to the transport of turbulent energy by the vertical component of the mean velocity.

4. The work done by mean viscous stresses, the work done by turbulent viscous stresses, and the dissipation due to the mean motion are all very small.

REFERENCES

1. Siao, T. T., "Characteristics of Turbulence in an Air-flow Model of the Hydraulic Jump." PhD dissertation, State University of Iowa, 1954.

2. Bakhmeteff, B.A., and Allan, W., "The Mechanism of Energy Loss in Fluid Friction" A.S.C.E. Transactions Vol. 111, 1946.

3. Rouse, H., Fluid Mechanics for Hydraulic Engineers, McGraw-Hill, 1938.

4. Hubbard, P.G., "A Constant-temperature Hot-wire Anemometer for the Measurement of Turbulence in Air," M.S. Thesis, State University of Iowa, 1949.

5. Arie, M., "Characteristics of Two-dimensional Flow behind a Normal plate in Contact with a Boundary on Half Plane" Memoirs of Faculty of Engineering, Hokkaido University, Vol. IV No. 2, Sept. 1956.

6. Einwachter, J., "Wasserwalzen und Energieumwandlung," Wasserwirtschaft und Technik, Jahrgang 1935, Hefte 29 und 30.

7. Goldstein, S., Modern Developments in Fluid Dynamics Vol. 1, Oxford Press, 1952.

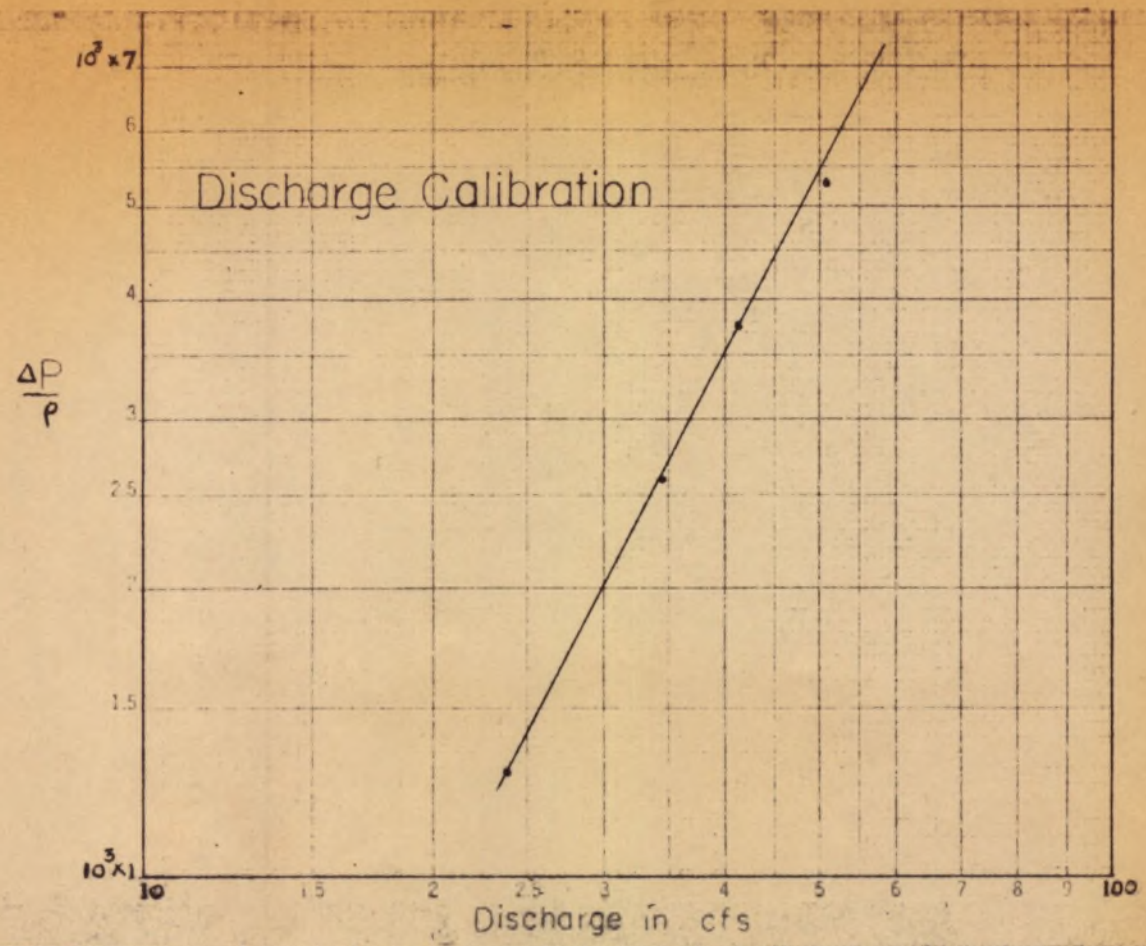

Fig. 1

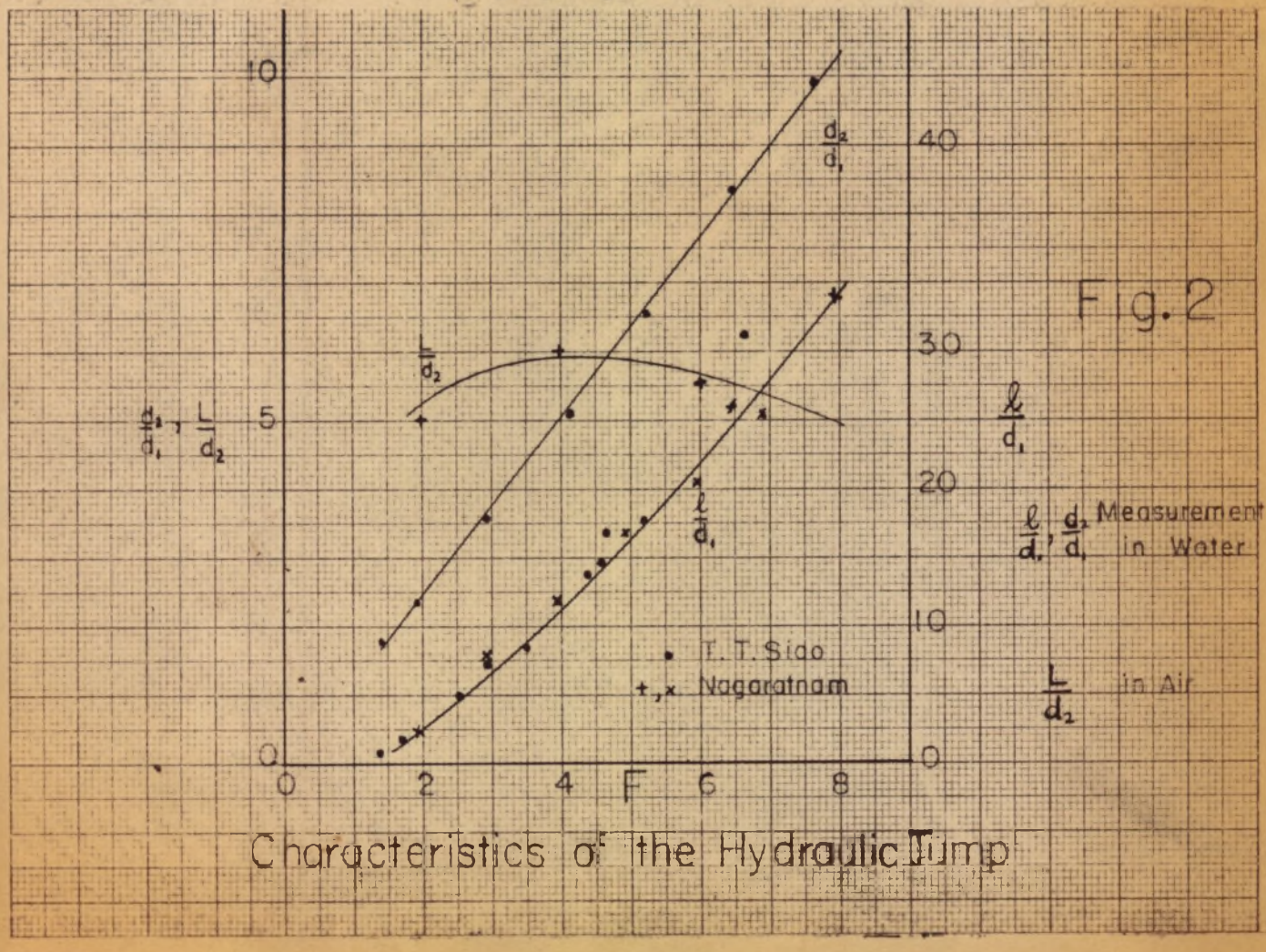

Fig. 2

Characteristics of the Hydraulic Jump

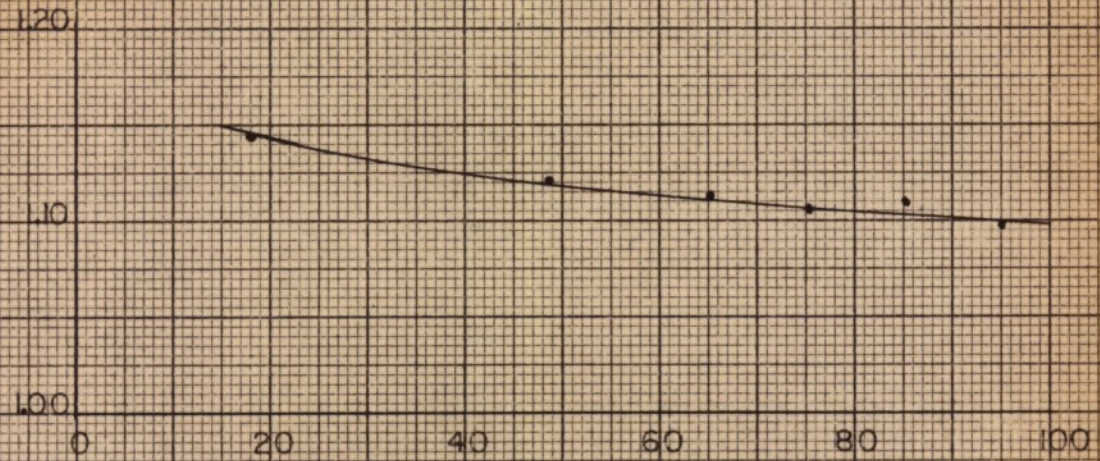

Fig. 3(a)

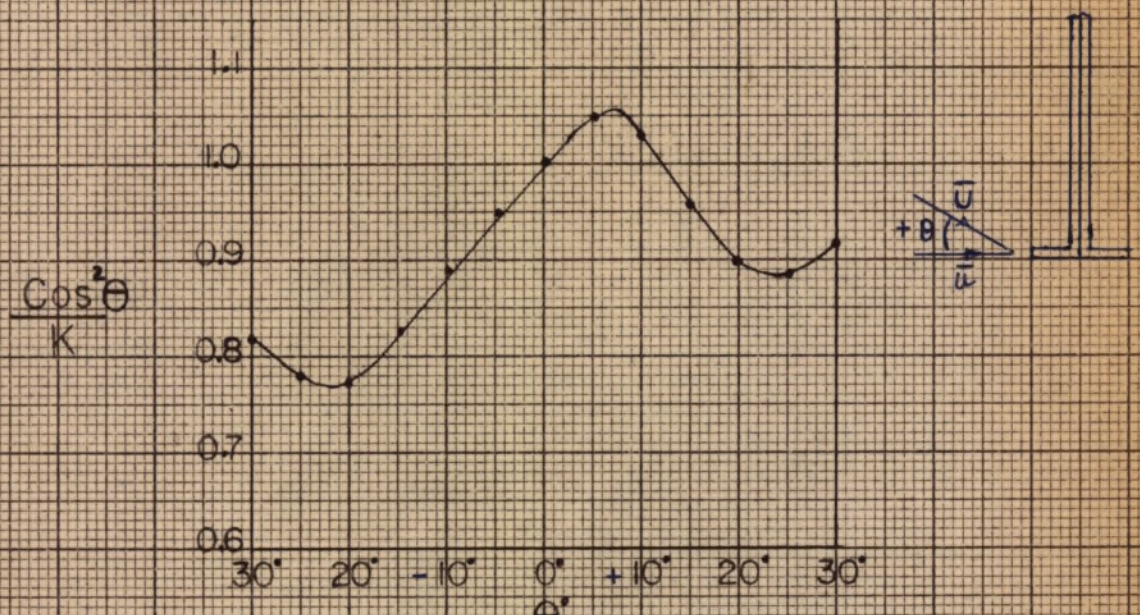

Fig. 3 (b)

Calibration of Pitometer

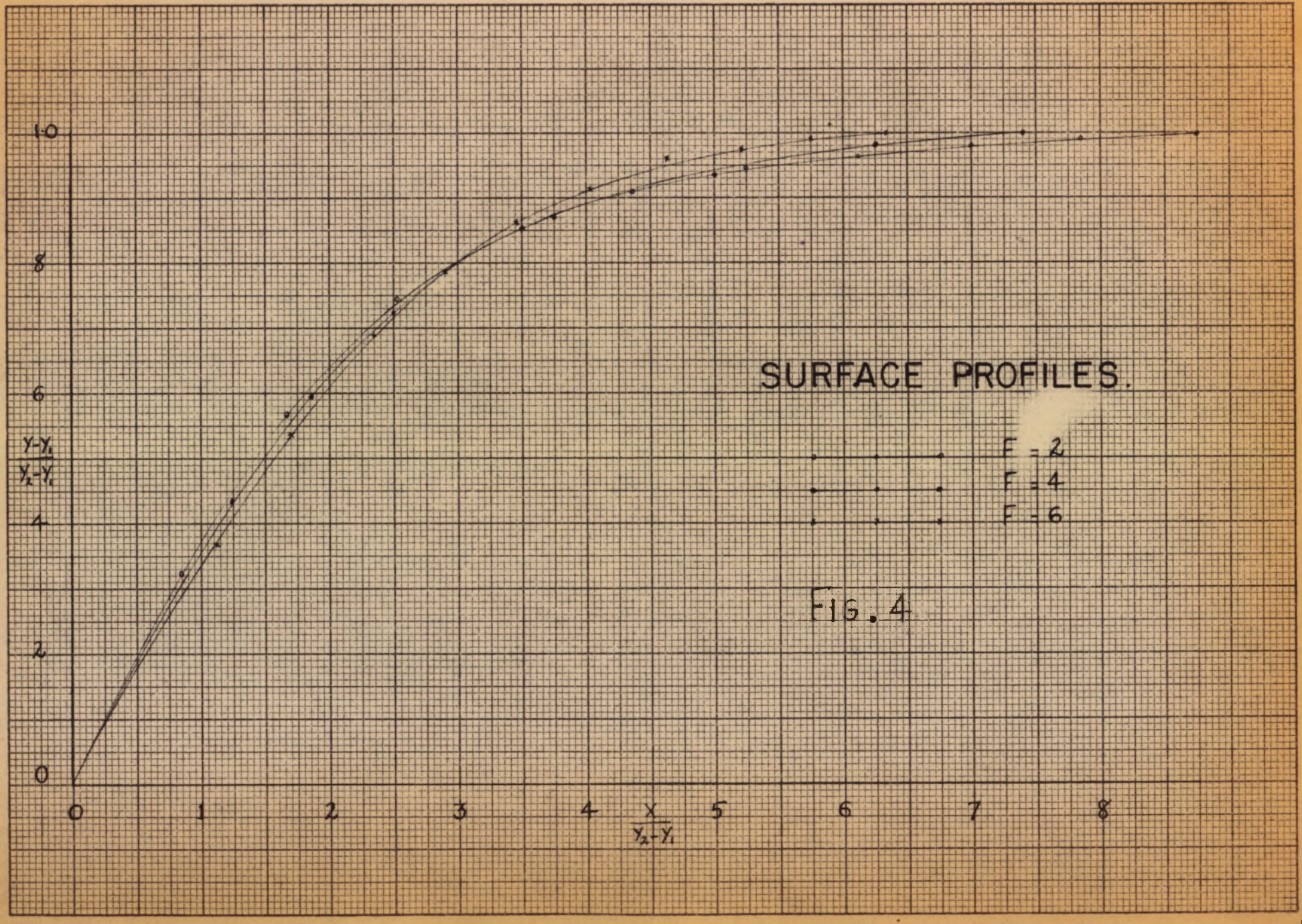
SURFACE PROFILES.
F = 2
F = 4
F = 6
1·0
8
6
4
2
0
$\frac{Y-Y_1}{Y_2-Y_1}$
0
1
2
3
4
5
6
7
8
$\frac{X}{Y_2-Y_1}$

Fig. 4.

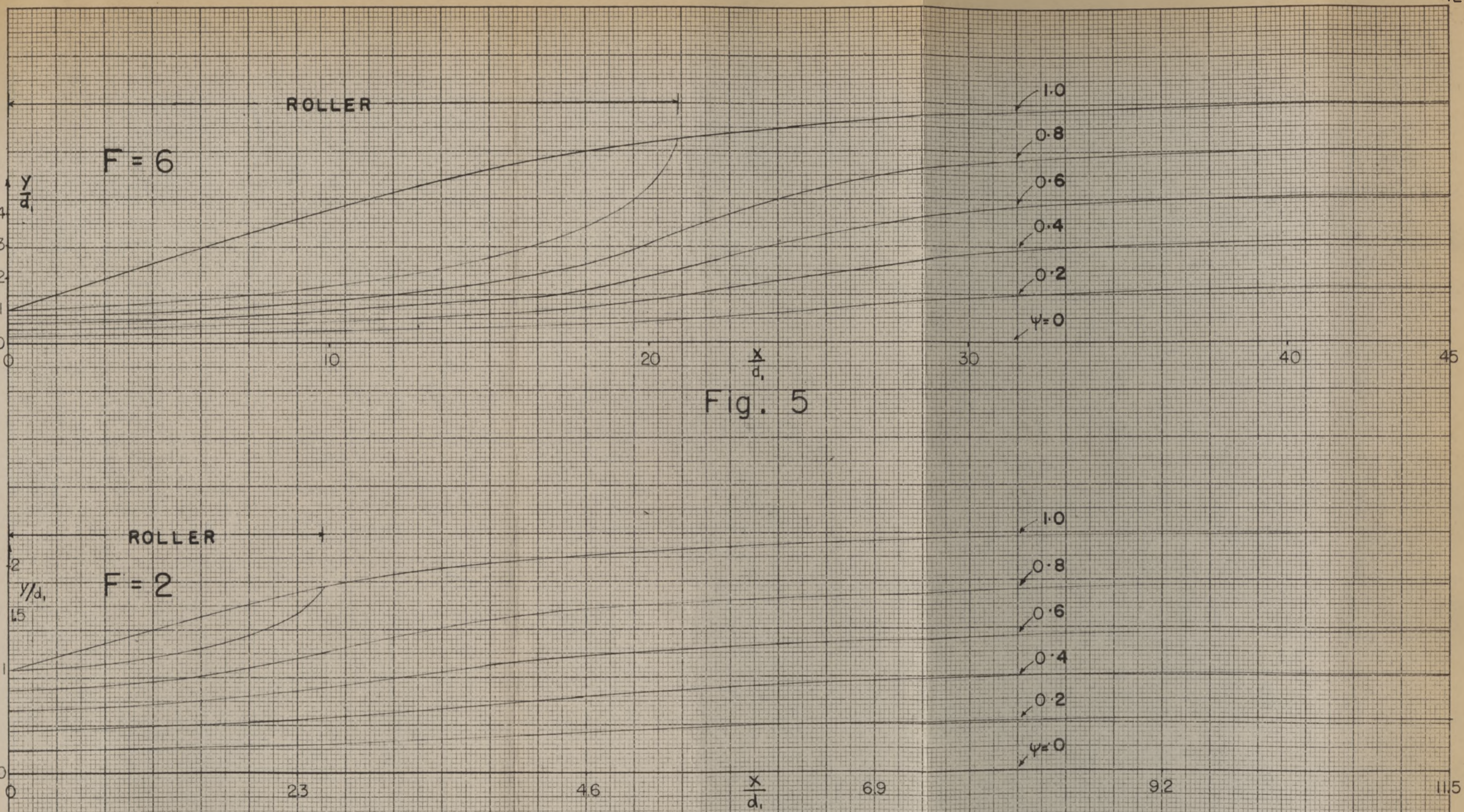

Fig. 5

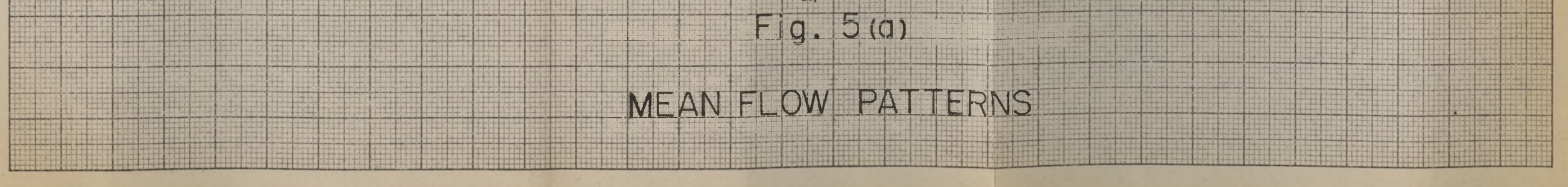

Fig. 5(a)

MEAN FLOW PATTERNS

$\frac{\bar{u}}{U_1}$ Profiles.

Fig. 6

F = 6

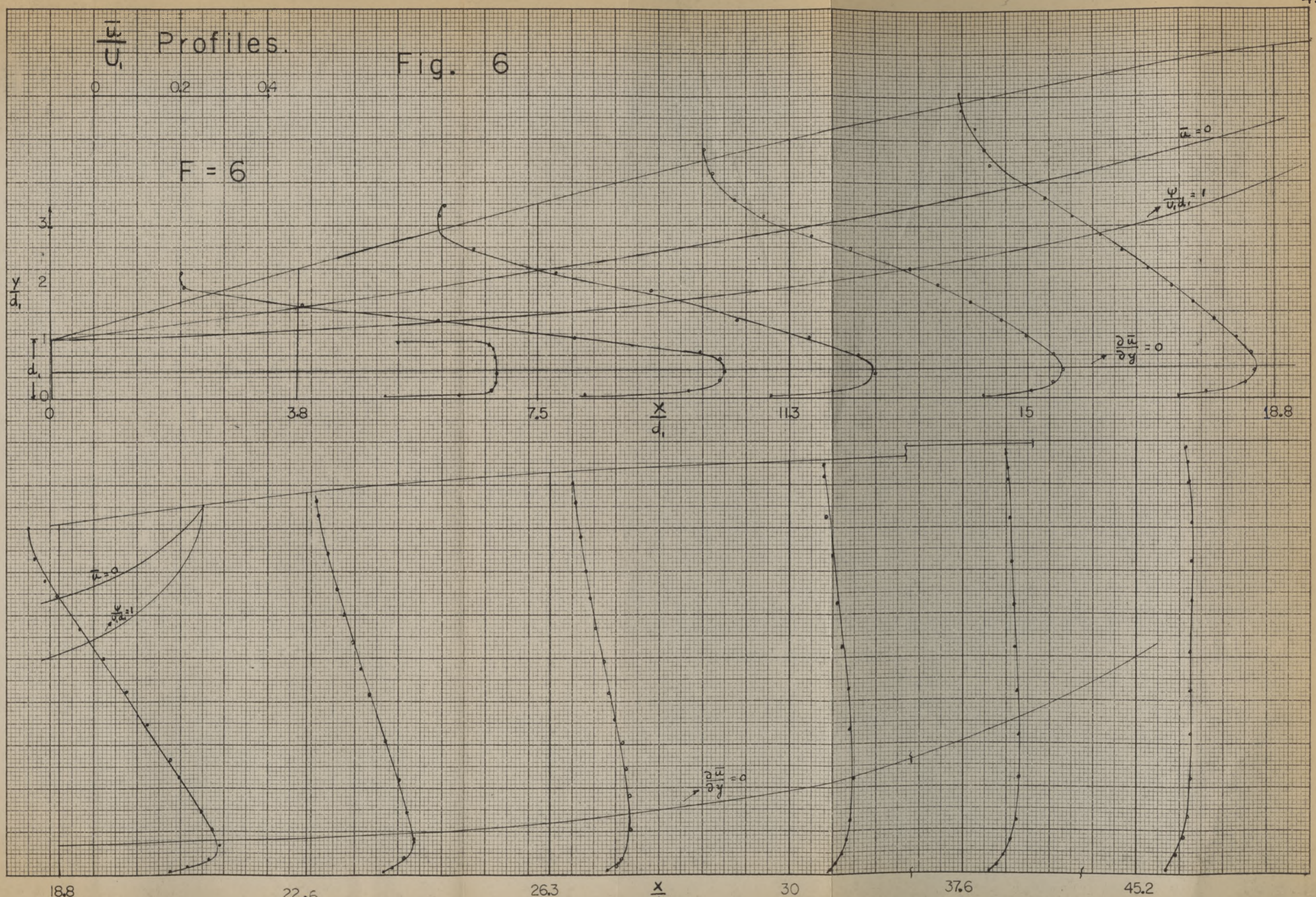

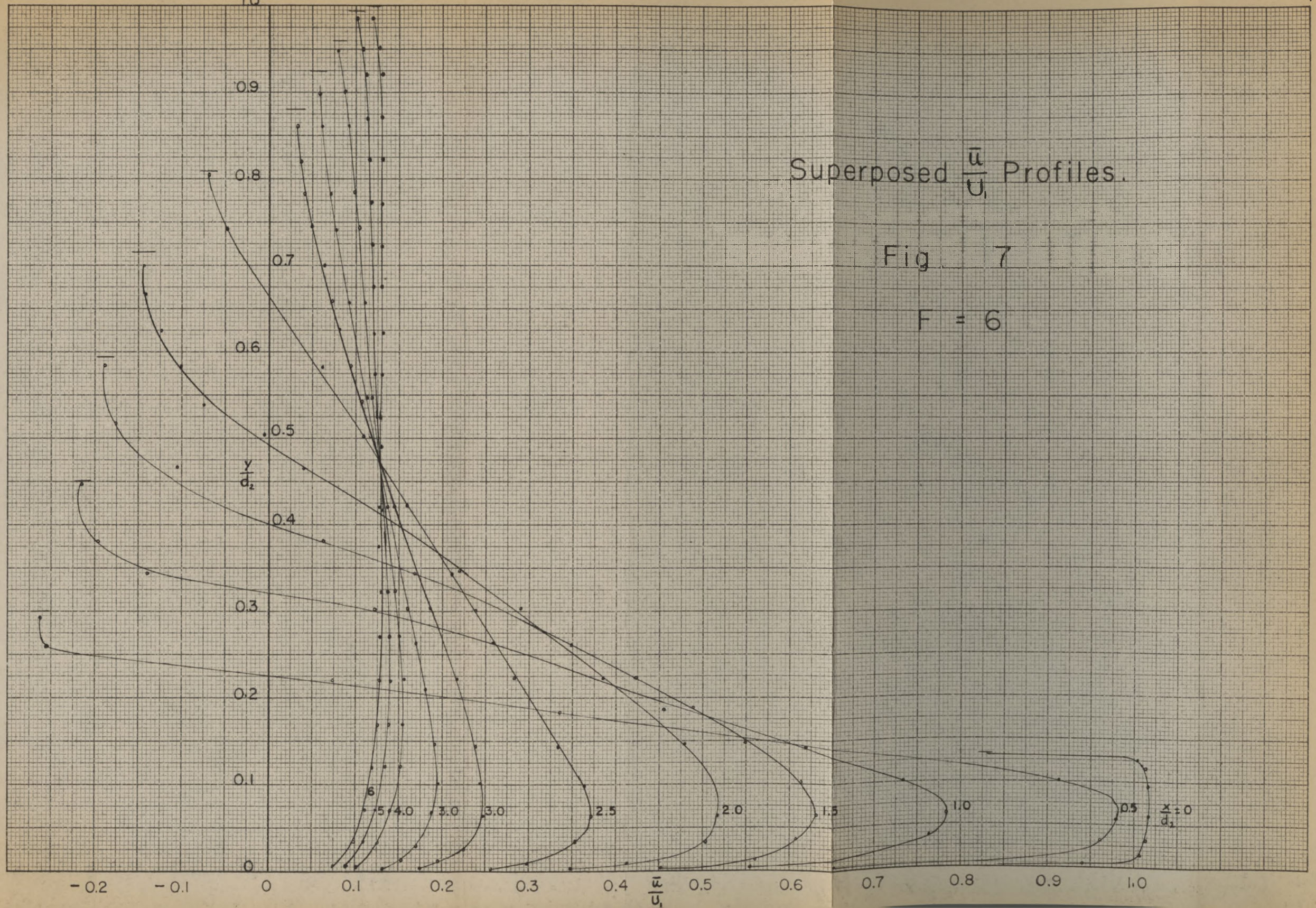

Superposed $\frac{\bar{u}}{U_1}$ Profiles.

Fig 7

F = 6

$\frac{\bar{v}}{U_1}$ Profiles.

Fig. 8

F = 6

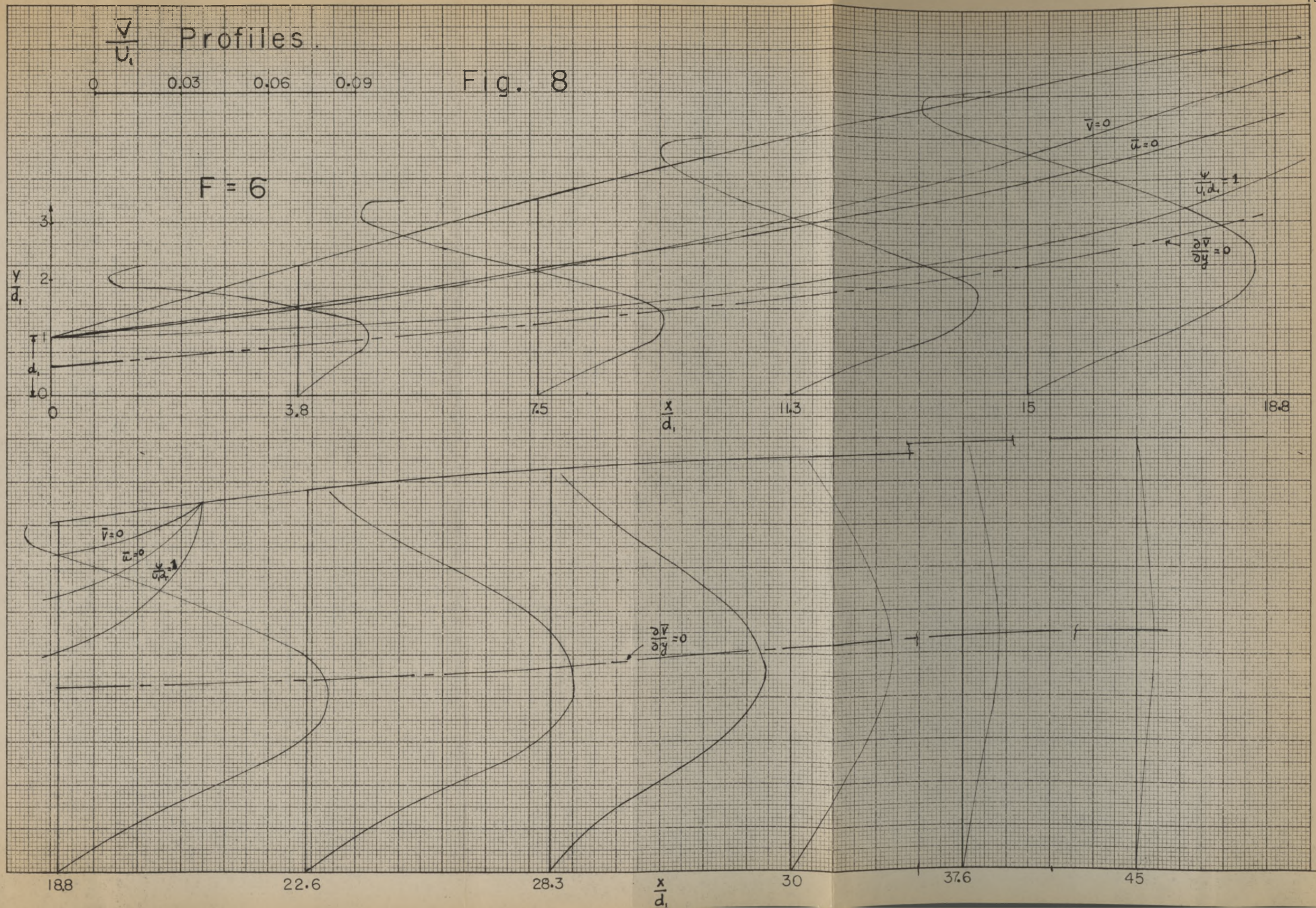

$\frac{\sqrt{u^2}}{U_1}$, $\frac{\sqrt{v^2}}{U_1}$ Profiles.

Fig. 9

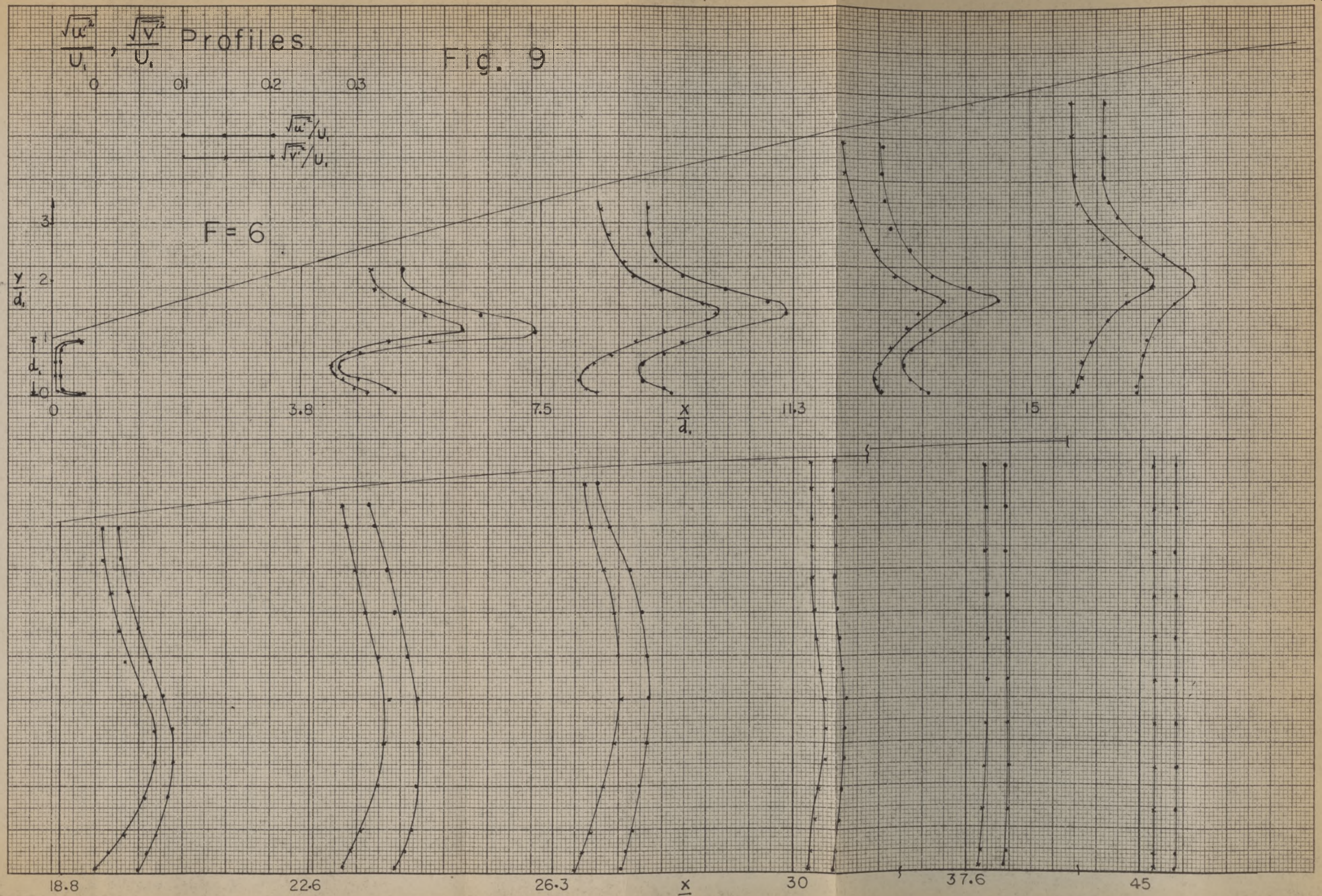

$\frac{\overline{u'v'}}{U_1^2}$ Profiles.

Fig. 10

F = 6

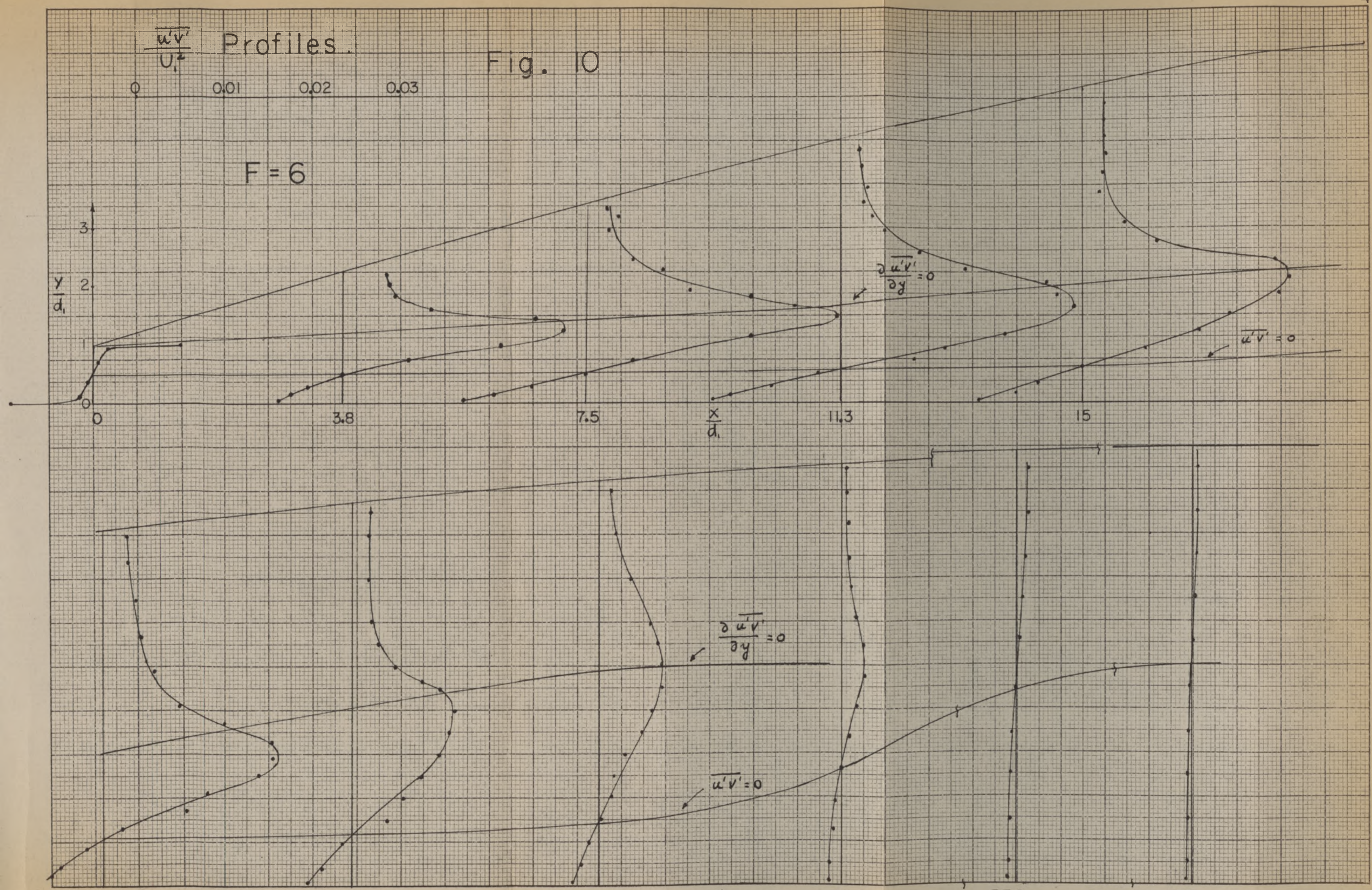

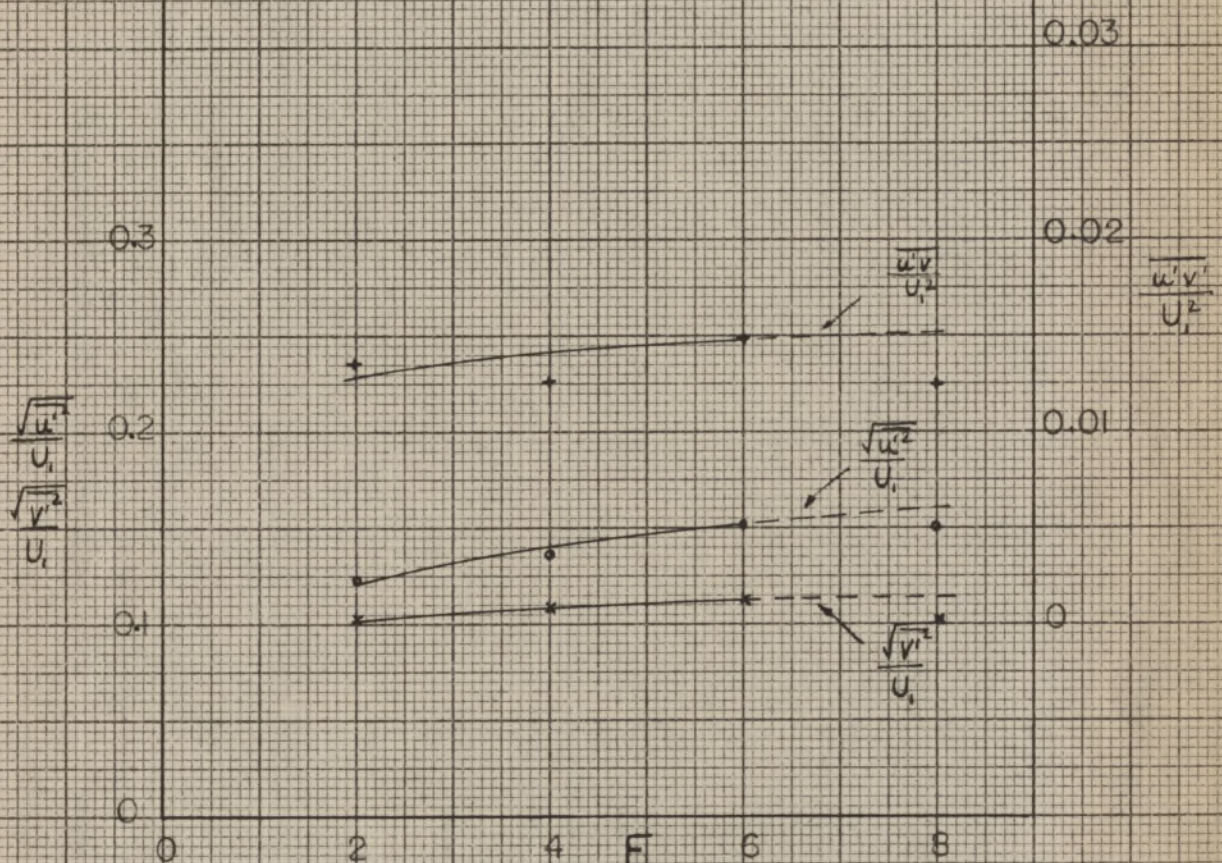

Characteristics of Turbulence in the Hydraulic Jump

(Average of Max. values of each Section used)

Fig. 11

Fig. 12

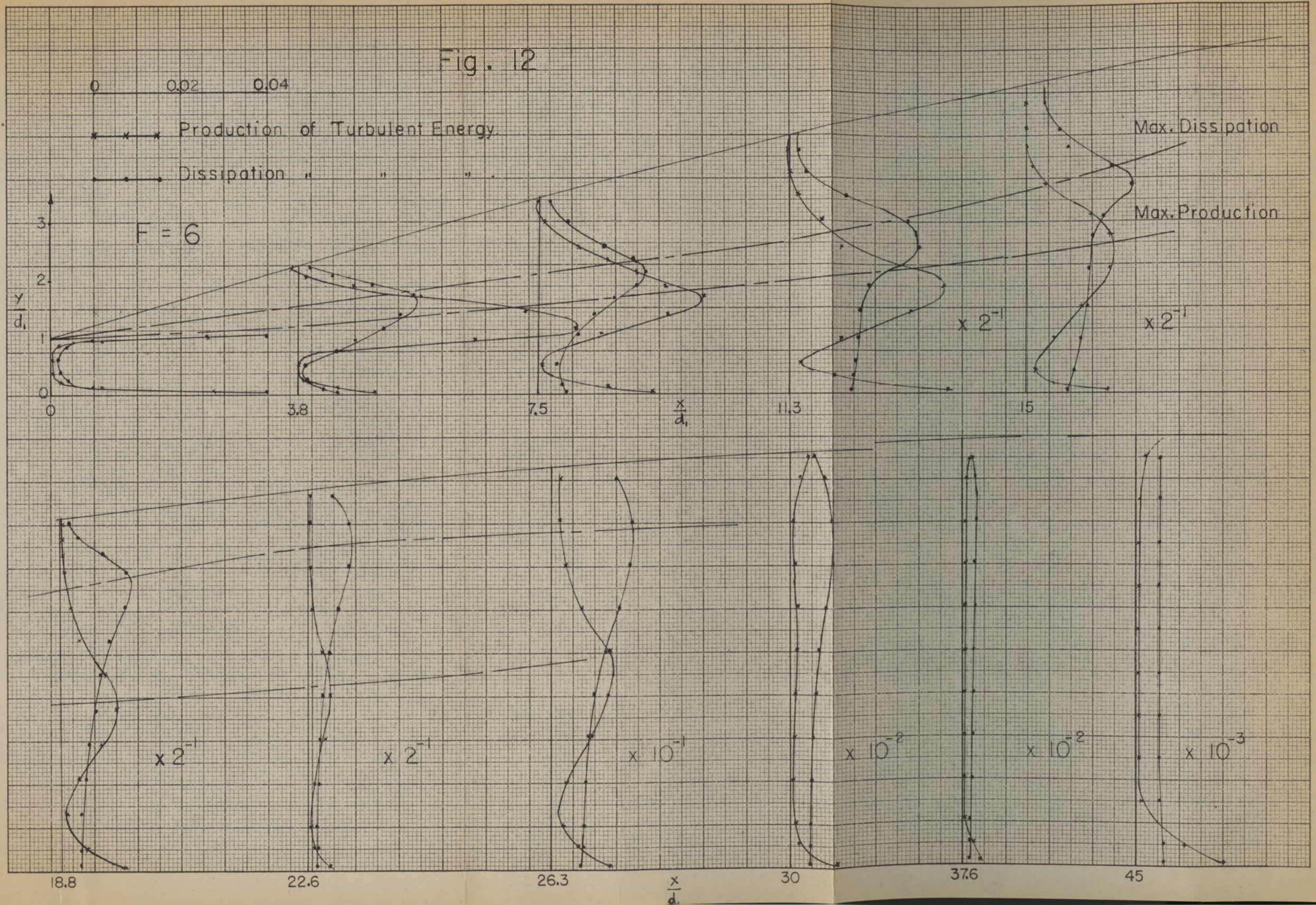
0 0.02 0.04
Production of Turbulent Energy.
Dissipation " " " .
F = 6
Max. Dissipation
Max. Production
y/d1
x/d1
0
3.8
7.5
11.3
15
18.8
22.6
26.3
30
37.6
45
x 2-1
x 2-1
x 2-1
x 10-1
x 10-2
x 10-2
x 10-3

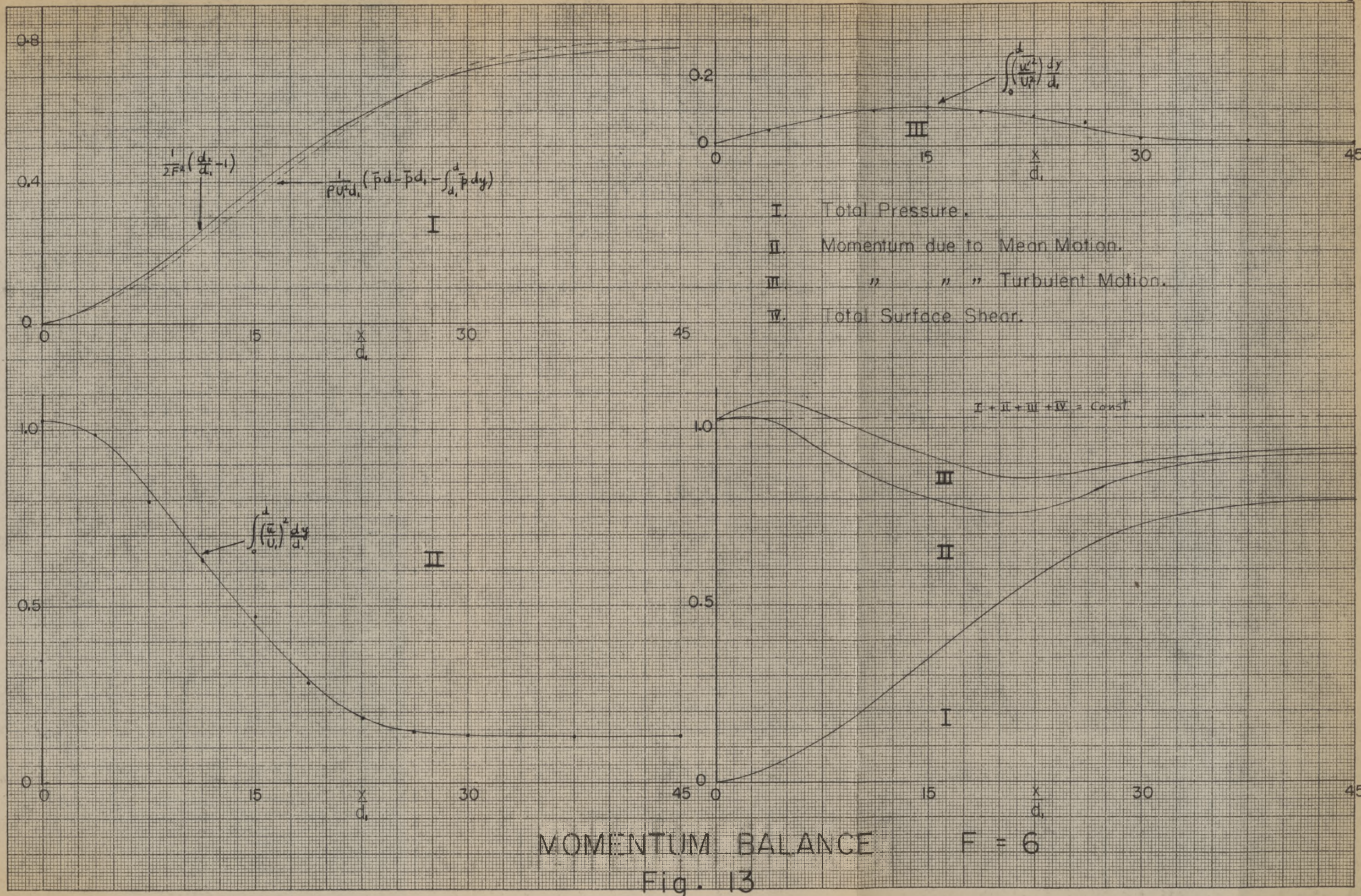

MOMENTUM BALANCE F = 6

Fig. 13

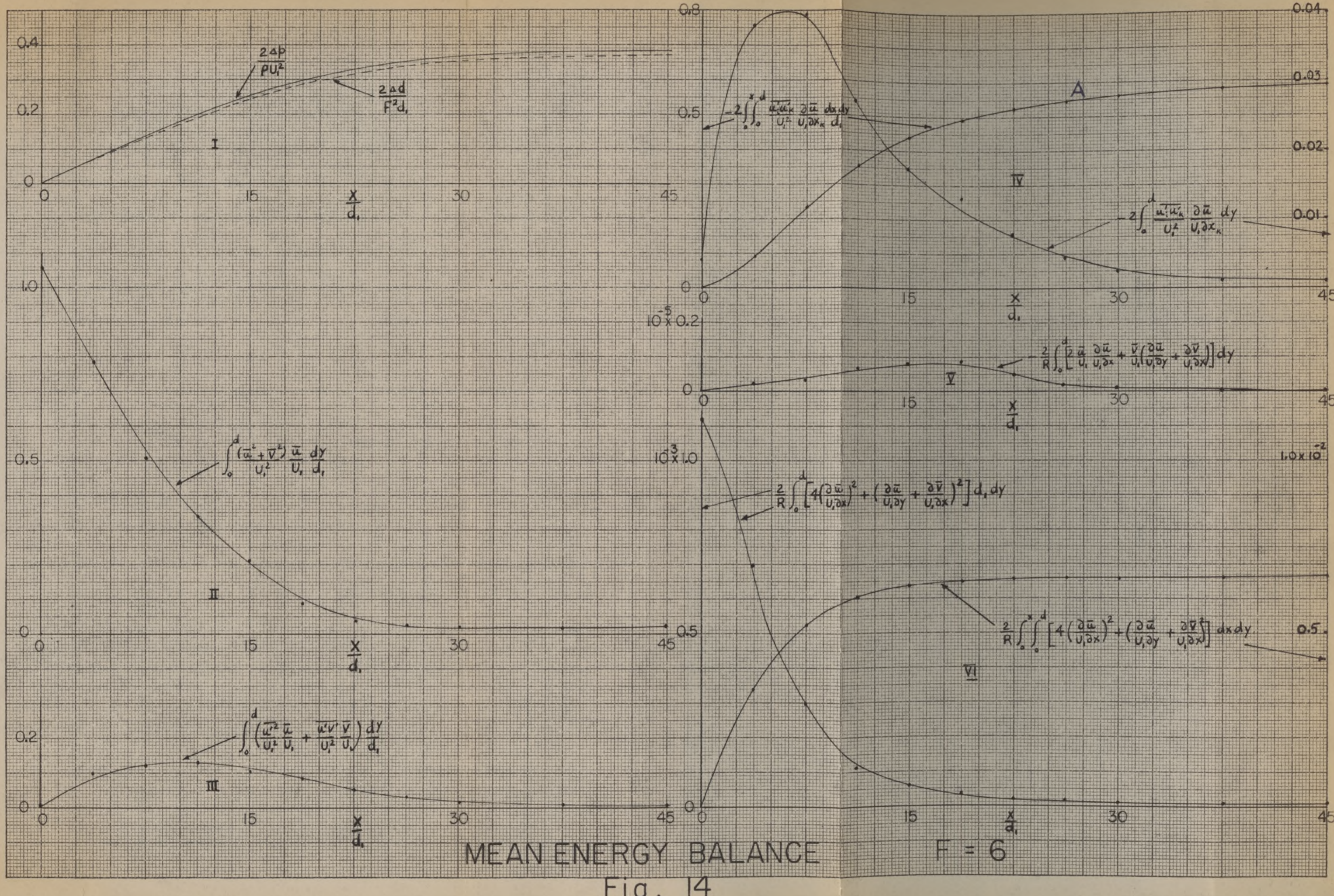

MEAN ENERGY BALANCE F = 6

Fig. 14

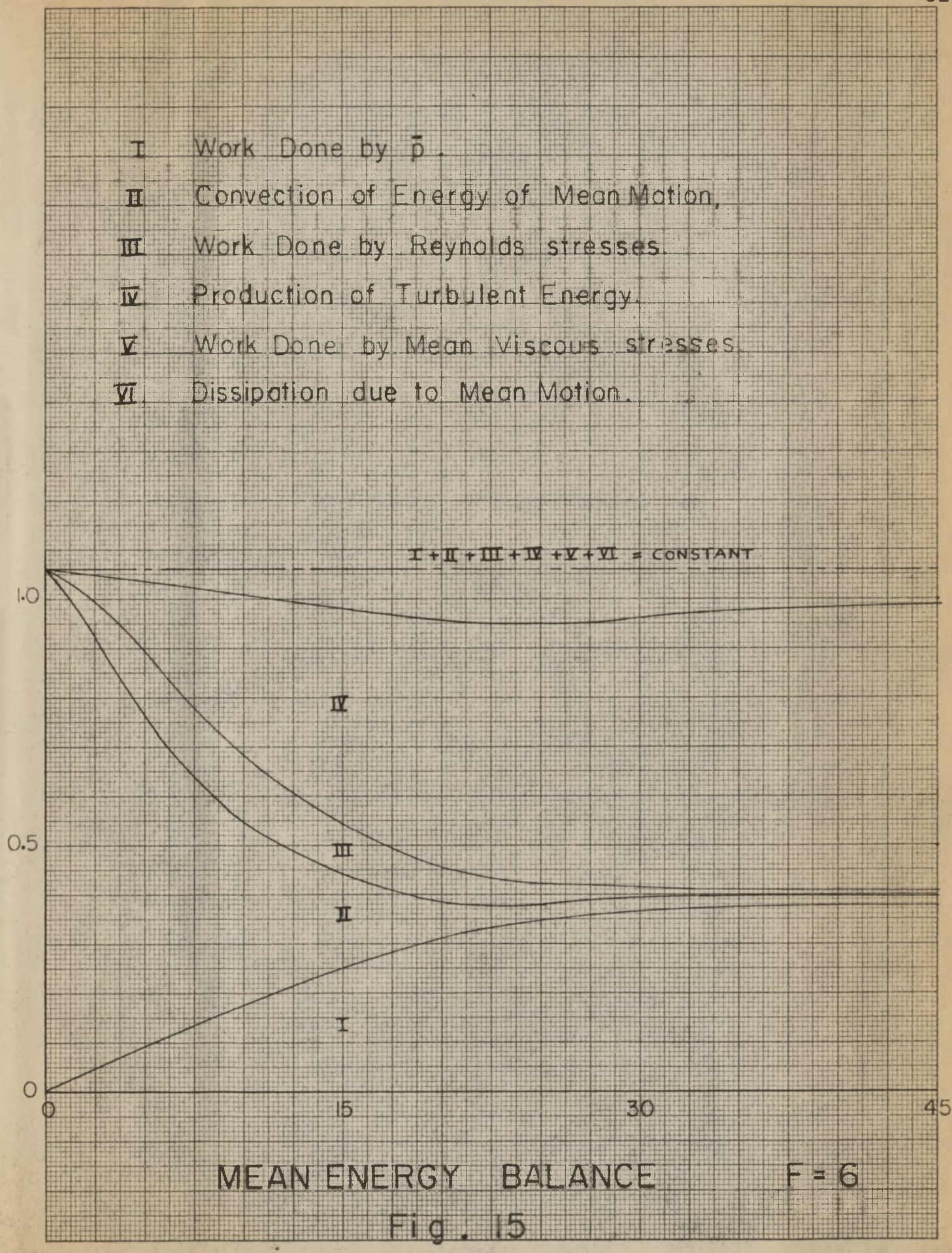

MEAN ENERGY BALANCE F = 6

Fig. 15

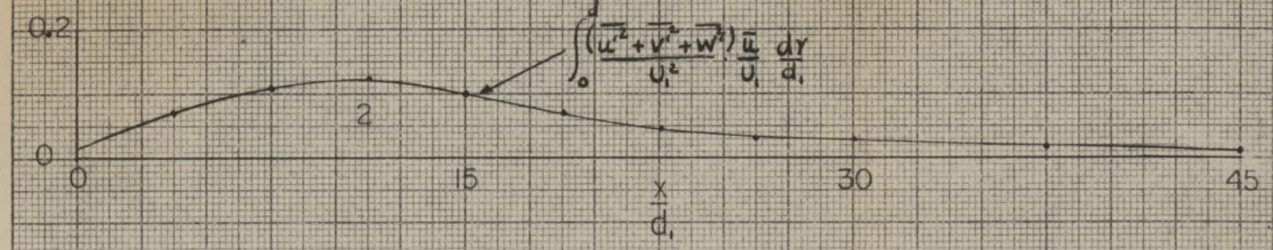

1. Work Done by p'.
2. Convection of Turbulent Energy.
3. Diffusion of " " .
4. Production of " " .
5. Work Done by Turbulent Viscous stresses.
6. Dissipation of Turbulent Energy.

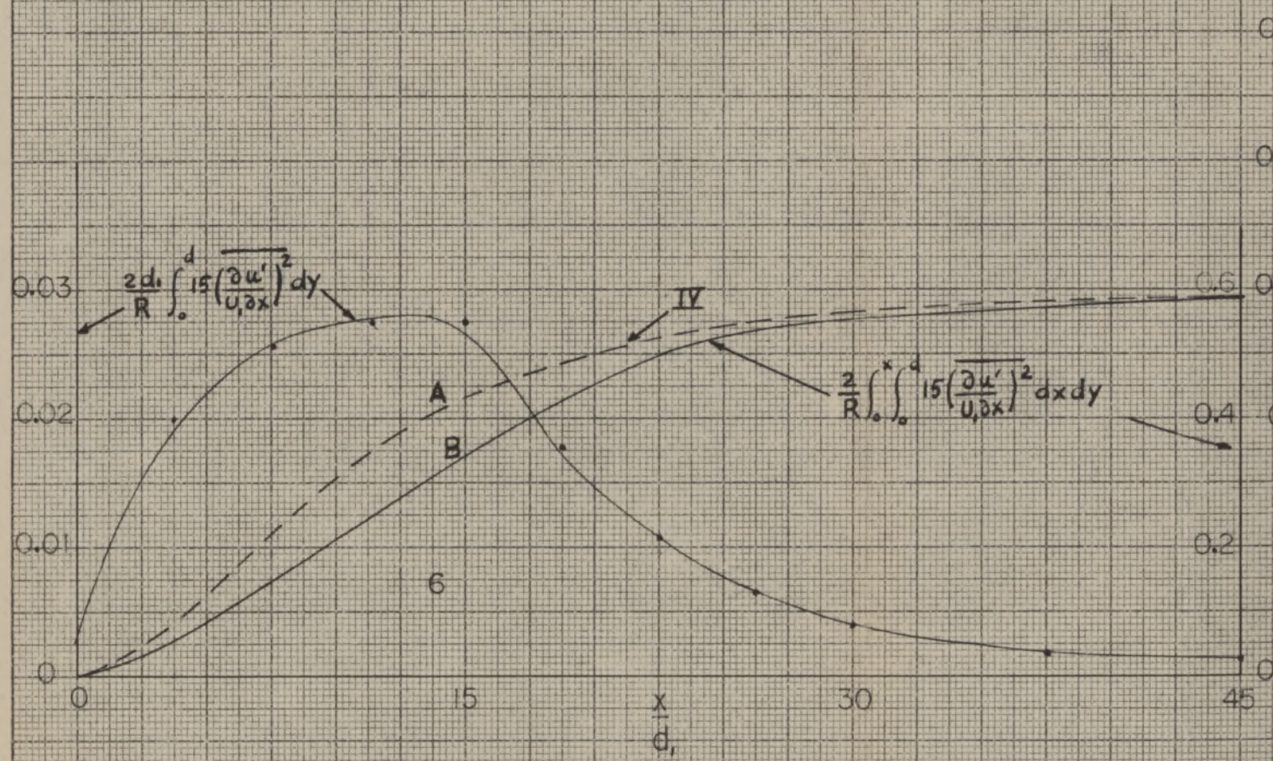

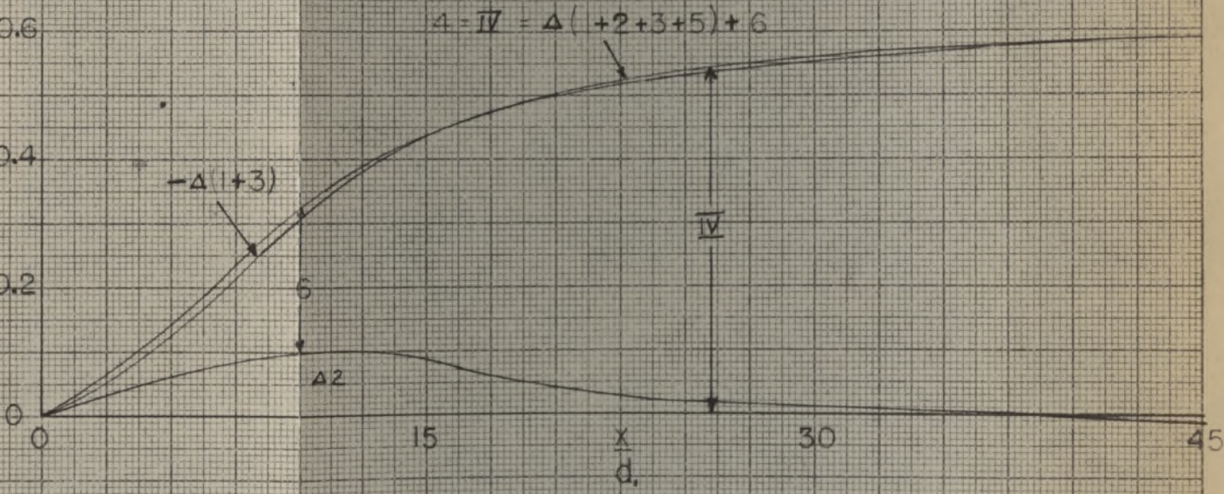

TURBULENT ENERGY BALANCE

Fig. 16

F = 2

$\frac{u}{U_1}$ Profiles. Fig. 6(a)

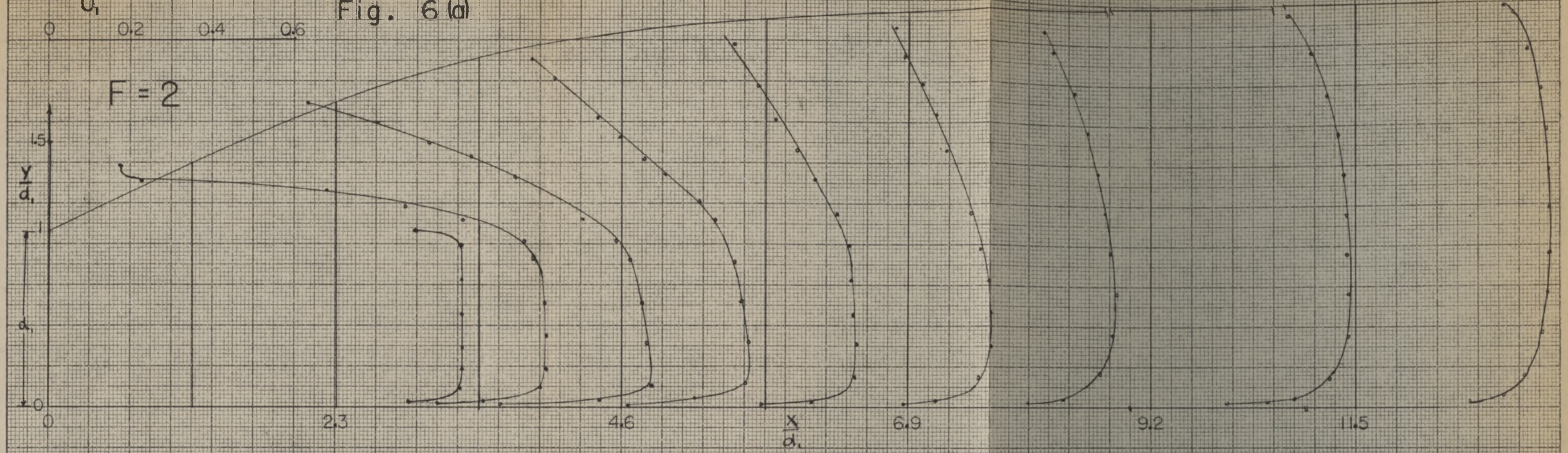

$\frac{v}{U_1}$ Profiles. Fig. 8(a)

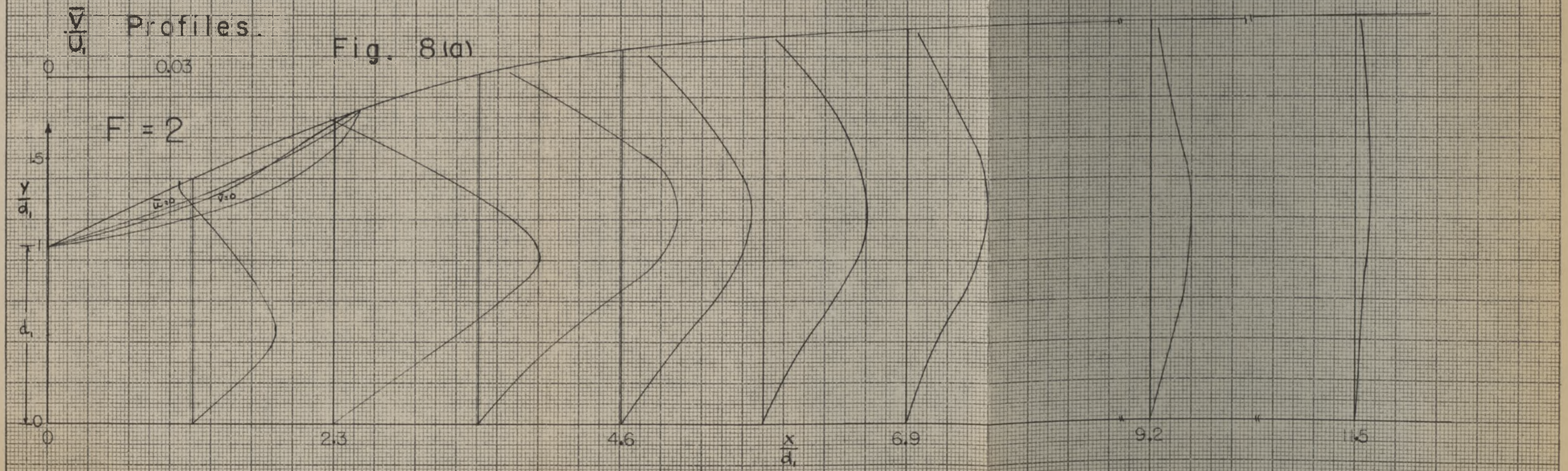

Superposed $\frac{u}{U_1}$ Profiles.

Fig. 7(a)

F = 2

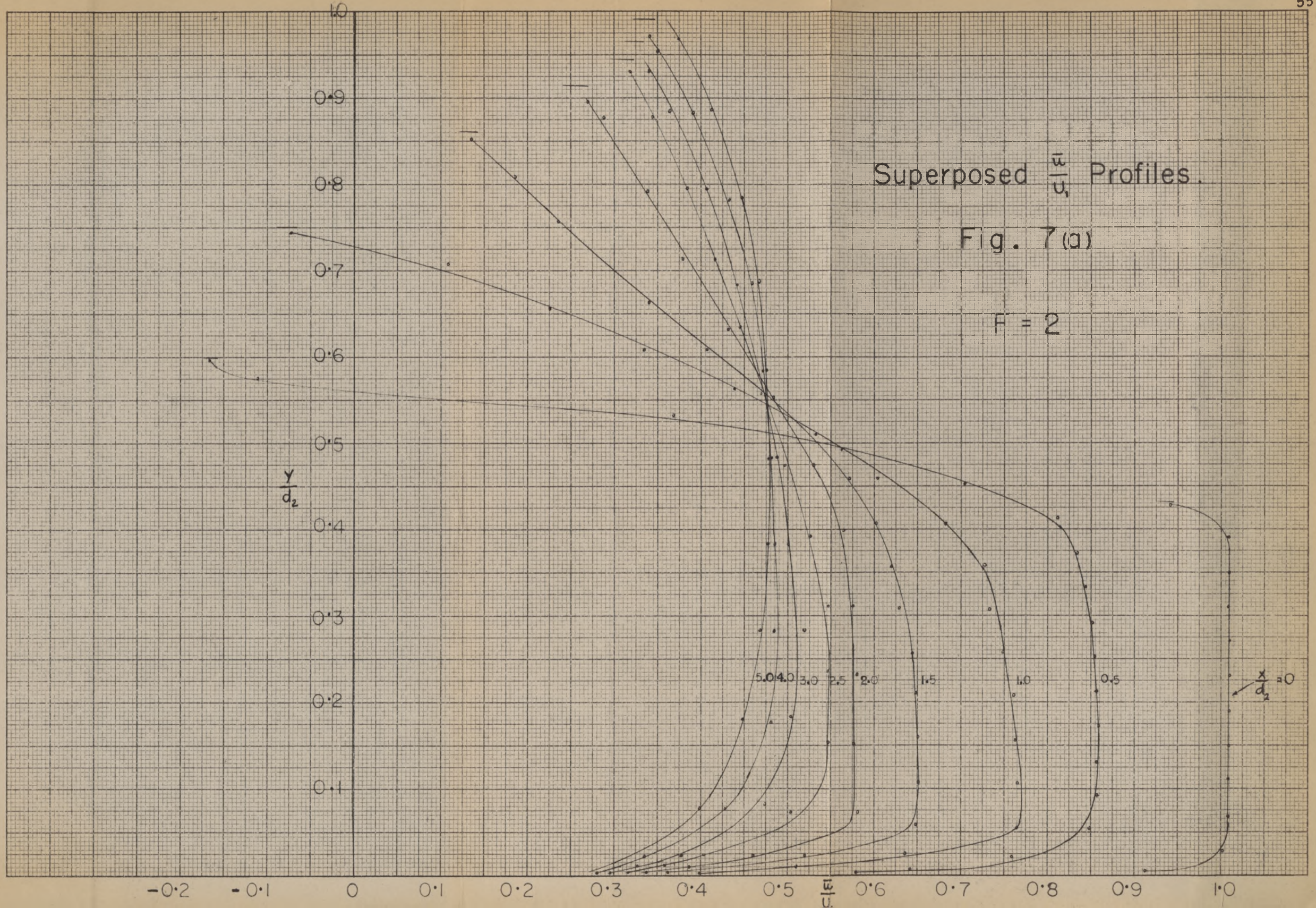

$\frac{\sqrt{u'^2}}{U_1}, \frac{\sqrt{v'^2}}{U_1}$ Profiles. Fig. 9(a)

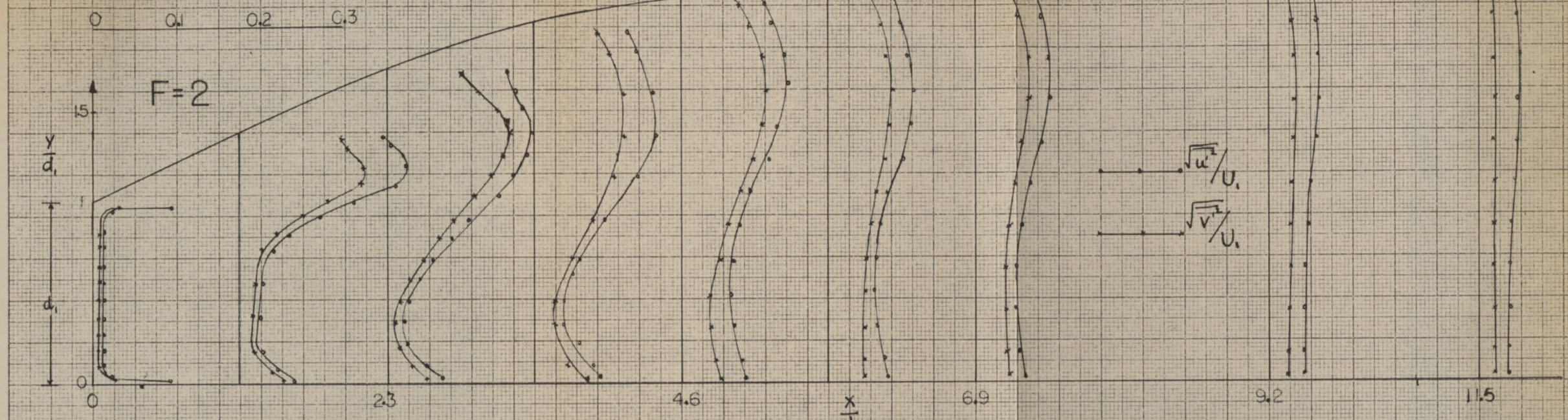

$\frac{\overline{u'v'}}{U_1^2}$ Profiles. Fig. 10(a)

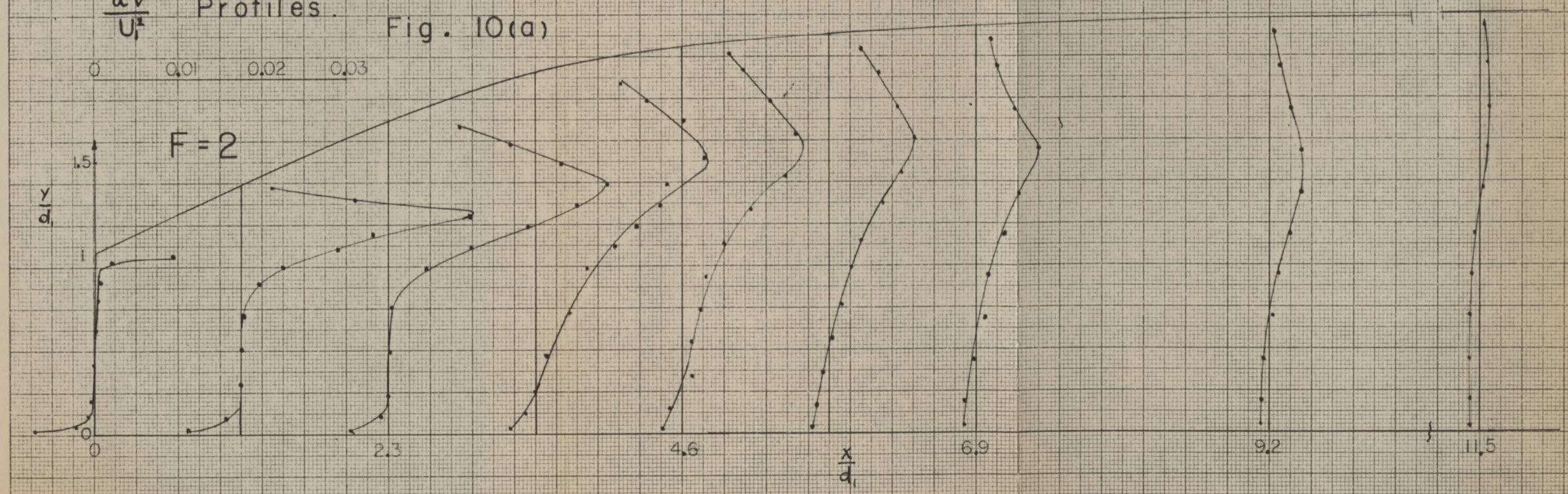

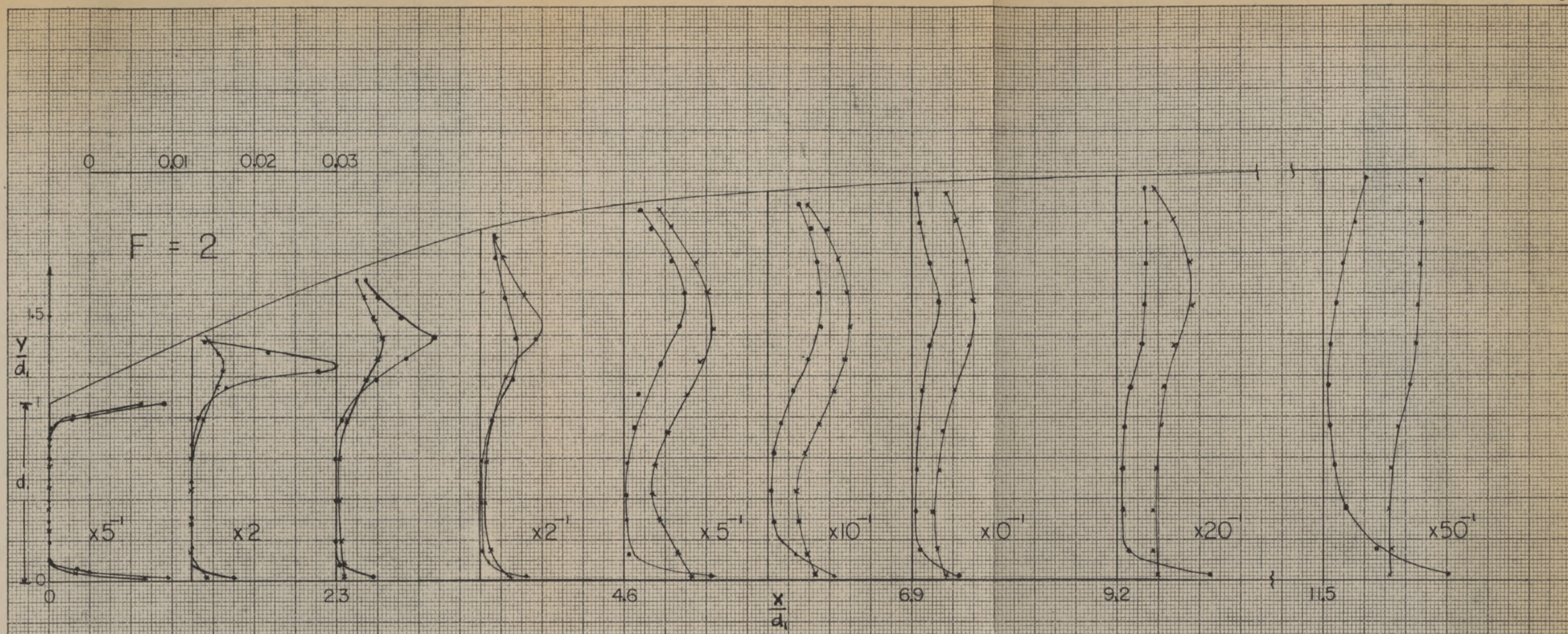
0
0.01
0.02
0.03
F = 2
1.5
y/d₁
1
d₁
0
x5⁻¹
x2
x2⁻¹
x5⁻¹
x10⁻¹
x0⁻¹
x20⁻¹
x50⁻¹
0
23
4.6
6.9
9.2
11.5
x/d₁
Production of Turbulent Energy.
Dissipation " " " "

Fig. 12 (a)

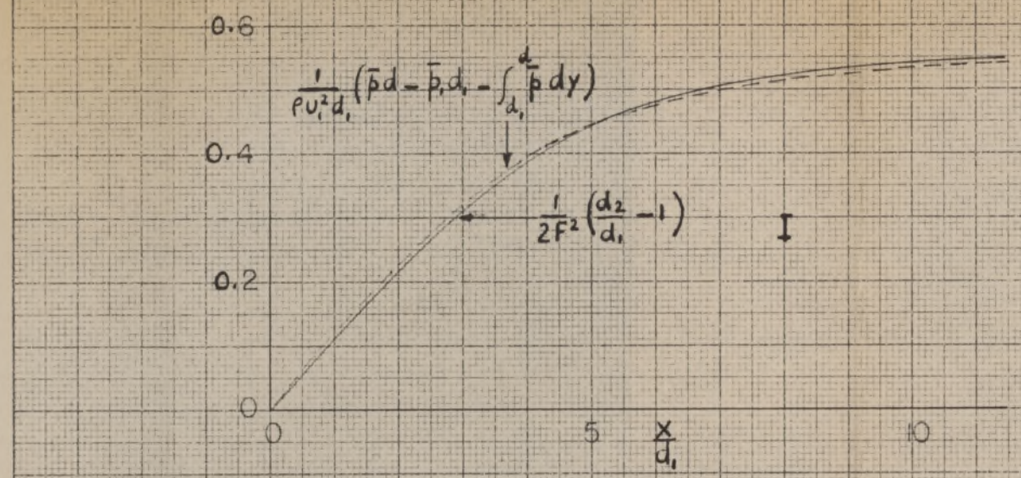

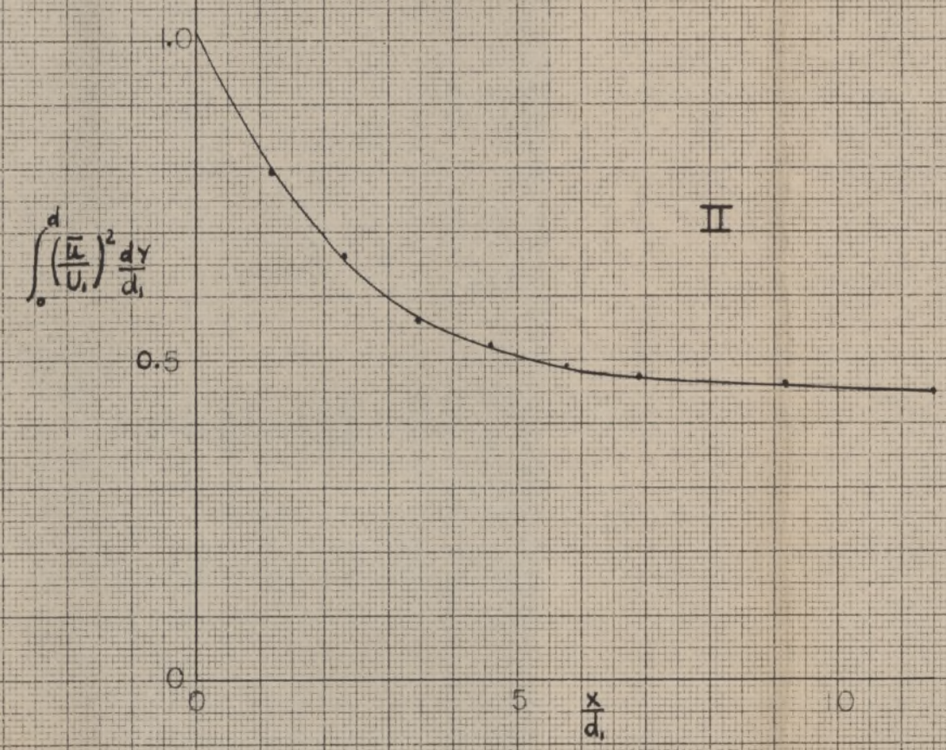

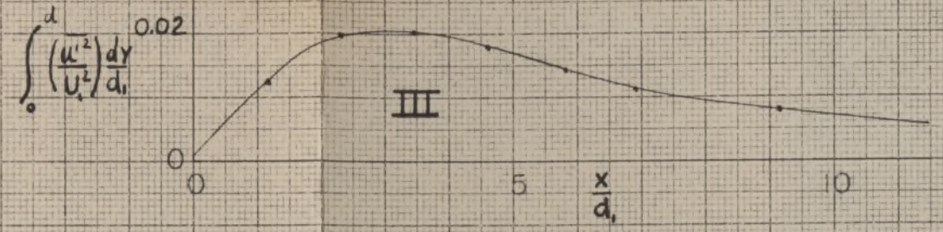

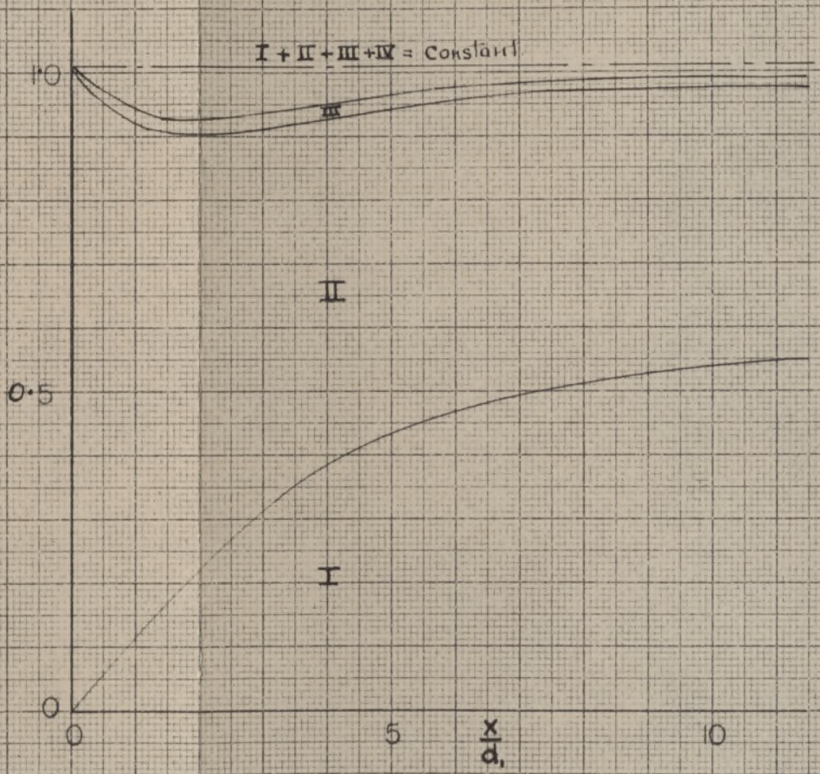

I. Total Pressure.

II. Momentum due to Mean Motion.

III. " " " Turbulent Motion.

IV. Total Surface Shear.

MOMENTUM BALANCE F = 2

Fig - 13(a)

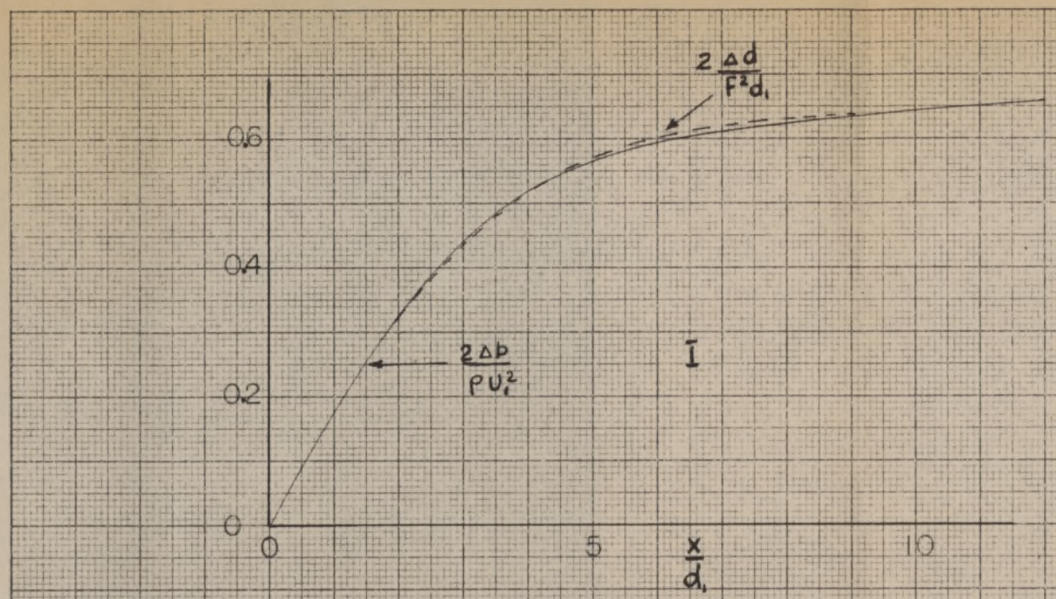

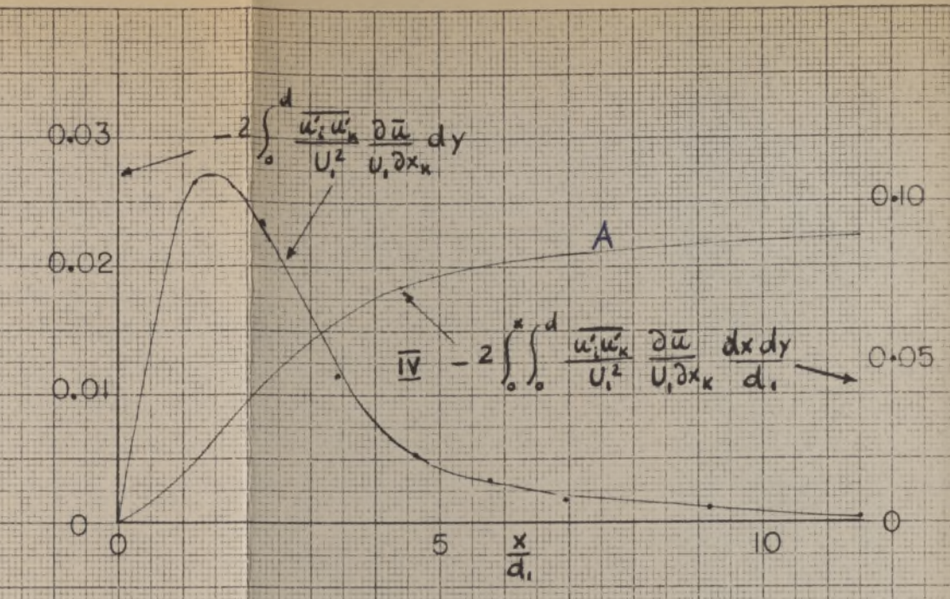

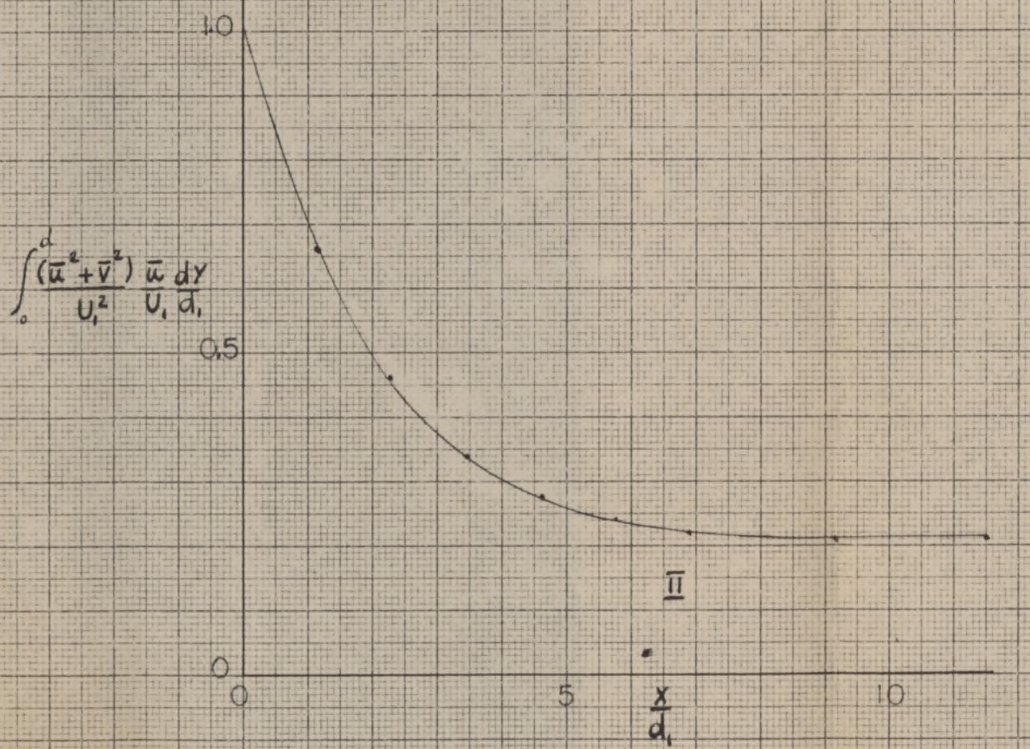

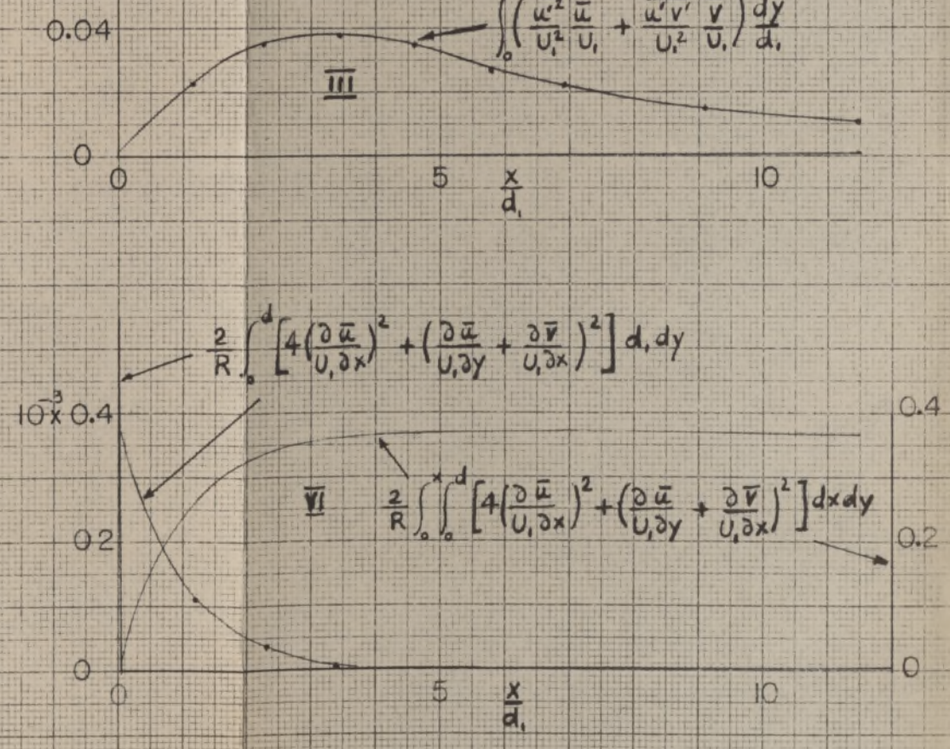

MEAN ENERGY BALANCE F = 2

Fig. 14 (a)

I. Work Done by $\bar{p}$.

II. Convection of Energy of Mean Motion.

III. Work Done by Reynolds stresses.

IV. Production of Turbulent Energy.

V. Work Done by Mean Viscous stresses.

VI. Dissipation due to Mean Motion.

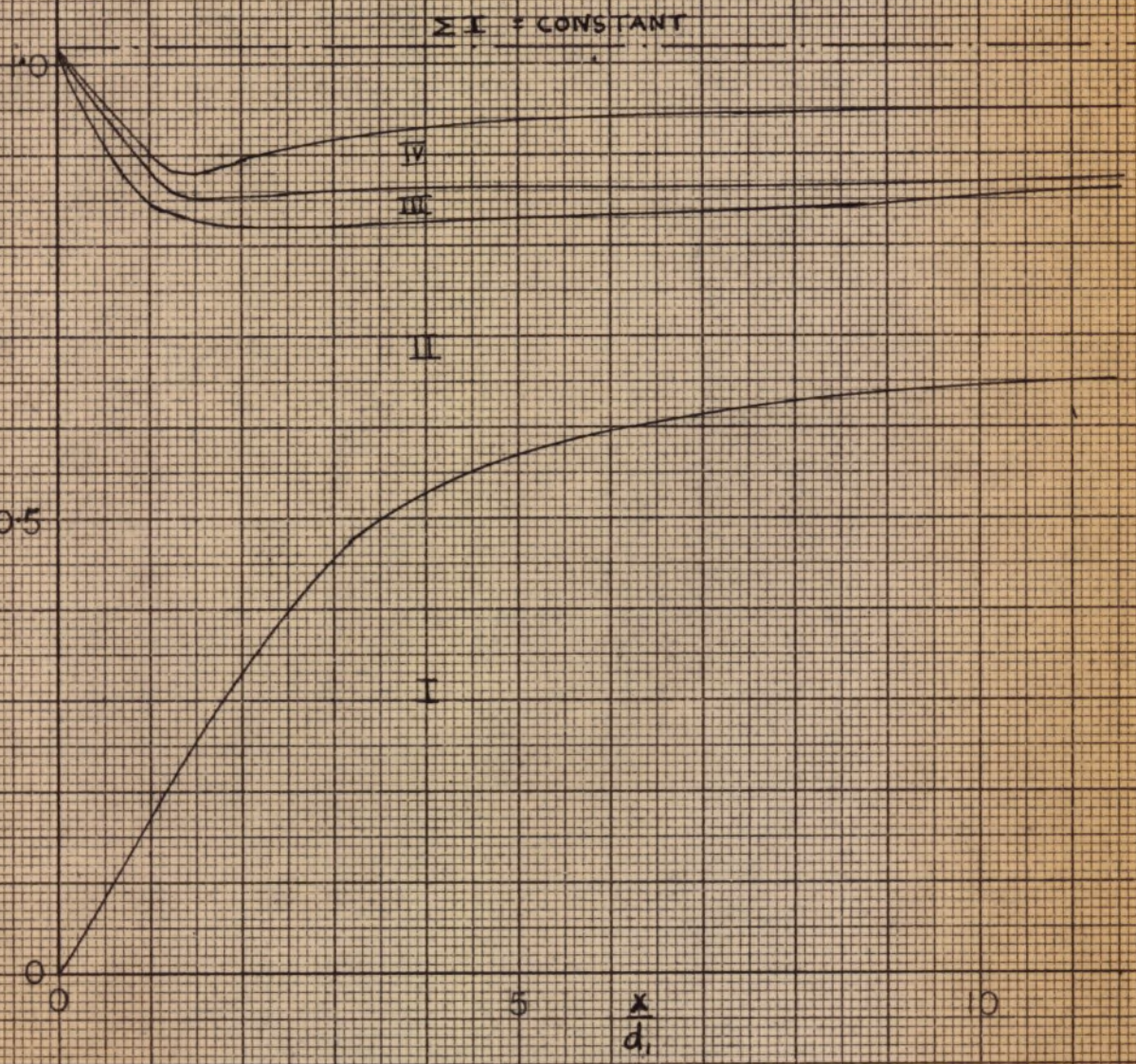

MEAN ENERGY BALANCE F = 2

Fig. 15 (a)

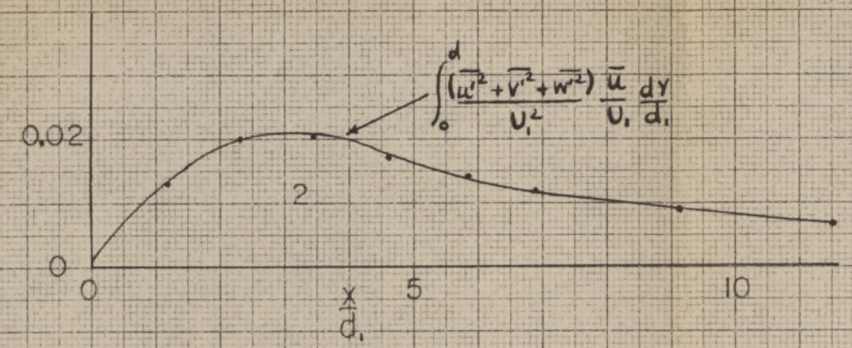

1. Work Done by p'.
2. Convection of Turbulent Energy .
3. Diffusion of " " .
4. Production of " " .
5. Work Done by Turbulent Viscous stresses.
6. Dissipation of Turbulent Energy.

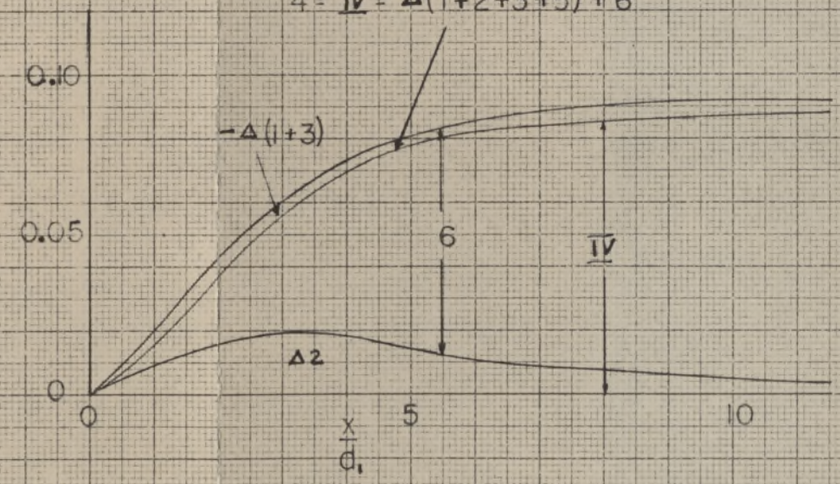

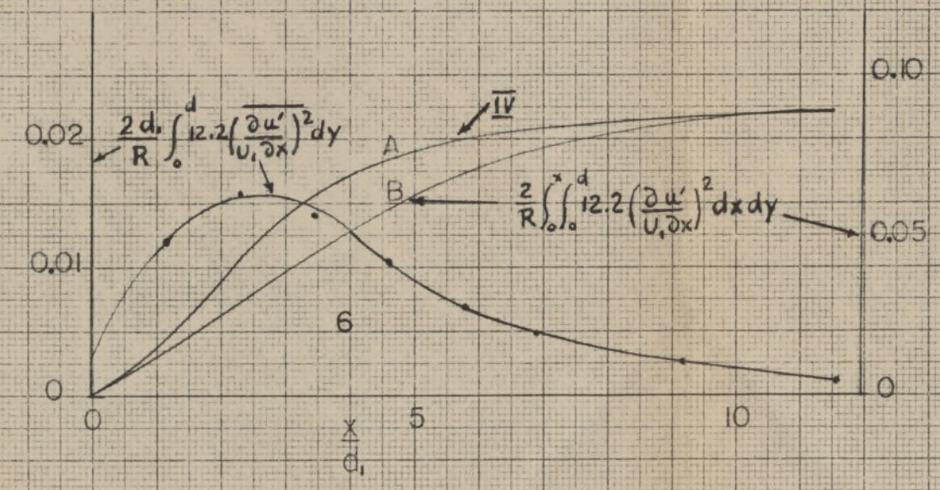

TURBULENT ENERGY BALANCE

Fig. 16 (a)
F = 2